Geochemical Journal, Vol. 48, pp. 527 to 547, 2014 doi:10.2343/geochemj.2.0348

# Simulating the D/H ratio of water formed in the early solar nebula

CARMEN TORNOW,[1]* PHILIPP GAST,[1] IVANKA PELIVAN,[1] STEFAN KUPPER,[1]
EKKEHARD KÜHRT[1] and UWE MOTSCHMANN[1,2]

[1]Institute of Planetary Research (DLR), Rutherfordstr. 2, 12489 Berlin, Germany
[2]Institute of Theoretical Physics, Technical University Braunschweig, Germany

(*Received January 23, 2014; Accepted November 6, 2014*)

Our solar system originated from a protoplanetary disk about 4.6 billion years ago. We simulate the formation of this disk by a three-stage model of the solar nebula (SN) which describes the hydrodynamic and chemical evolution of a cold cloud core consisting of gas and one mass percent dust. Considering the first two stages of this SN-model we have studied the formation and deuteration of water, which is an important precondition of life.

During the quasi-stationary stage of the cloud core, corresponding to the first SN stage, water has been formed on the surface of dust grains by the hydrogenation of oxygen. The gas and dust temperatures, which differ at the outer boundary of the core, are nearly 14 K and reach 9 K in its center. Therefore an icy mantle forms on the dust grains in less than $10^5$ years and changes slowly afterwards. Because of the large abundance of hydrogen and a carbon to oxygen (C/O) ratio of 0.44 the major component of this mantle is water ice. We found that the water produced in the gas phase amounts to less than 20 ppm of the water formed on dust grains. In both phases, the deuterium enrichment $\delta$D (‰) relative to the Standard Mean Ocean Water varies at 1 AU from 15,050 to 63,100‰ (or a D/H ratio from 2 to 0.5%) and indicates the low formation temperature of water molecules.

In the second stage of our SN-model, the collapse of the cold cloud core is simulated using a semi-analytical solution of the magneto-hydrodynamic equations. Due to relatively high temperatures around the center ($10^{2-3}$ K), this range is identified with the hot corino observed in regions of low mass star formation in our galaxy. There, the icy mantles of the grains vanish due to desorption of water molecules from their surfaces. As a result the water to hydrogen ratio in the gas phase increases to $10^{-5}$–$10^{-4}$. Since this water was formed in a cold region and a collision related destruction of water molecules (occurring at ~$10^5$ K) can be neglected everywhere except for the protostellar source in the core center (<$10^{-2}$ AU), the deuterium enrichment in the outer hot corino (1 AU) reaches $\delta$D of 2,210‰ (or D/H of 0.1%) at the end of the main collapse phase. Different reasons for this high value are discussed.

Keywords: collapsing core, solar nebula, dust chemistry, D/H ratio of water

## INTRODUCTION

The formation of low-mass stars is observable in the large hydrogen clouds located in a region from nearly 50 pc above to 50 pc below the central plane of our galaxy. Surveys of these large dark or even giant molecular clouds show that they have an inhomogeneous structure of filaments which themselves consist of dense cores surrounded by diffuse inter-core matter (André, 2013). The main fraction of these cores form low-mass stars if one assumes that the mass distribution of new born stars is similar to the one of field stars and considering that nearly 99% of field stars have a stellar mass ≤1.4 $M_O$ (LeDrew, 2001; Lada, 2006), where $M_O$ denotes the solar mass. Observations of the Chamaeleon molecular cloud give rise to the assumption that starless cores can be in a collapsing prestellar or in an unbounded stage while protostellar cores contain relatively hot hydrostatic gas-dust spheres—the precursors of T-Tauri stars—and outflows (Belloche *et al.*, 2011a, b). After a time between $10^5$ and $10^6$ years the gaseous envelope disappears and a T-Tauri star surrounded by a turbulent disk becomes observable.

Our SN-model is based on these three stages of low-mass star formation (Fig. 1). Its early part simulates the starless stage as a quasi-stationary cloud core and the protostellar stage as a collapsing cloud core. The material in each stage consists of the gas phase with about 99% of the total core mass and the dust phase. Both phases interact with each other thermally and chemically. The energetic equilibrium of the first stage corresponds to a spherical core constructed by Bonnor (1956) and Ebert (1957). Since a number of these cores are characterized by oscillations (Keto *et al.*, 2006), which are mathematically similar to stellar pulsations, relatively long lifetimes

*Corresponding author (e-mail: carmen.tornow@dlr.de)

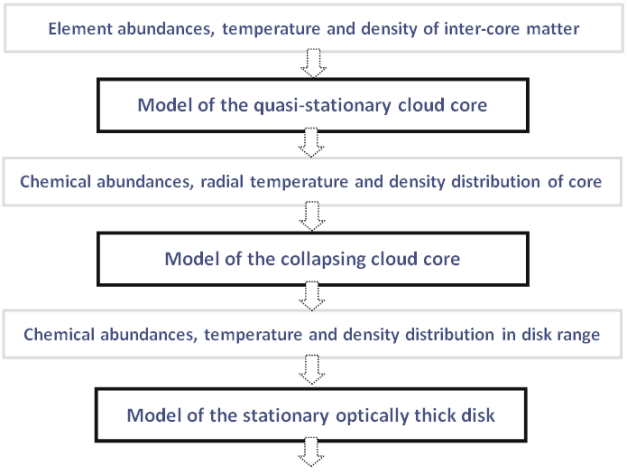


*Fig. 1. Flow chart of the SN-model consisting of three stages (boxes with black boundary), where the first and second stages are combined to model the early SN (see introducing text). The third stage, constructed by a rotating geometrically thin disk, is considered as late SN. Online version of this paper contains color figures.*

(>3 Myr) are realistic and would explain the low conversion rate of stars from cloud cores. However, rapid formation of low-mass stars due to a short period of the starless core stage cannot be ruled out (Visser *et al*., 2002). Consequently, the lifetime of the quasi-stationary core is not well constrained and values varying between 1 and 6 Myr are likely. According to Bacmann *et al*. (2000), starless cores have nearly flat radial density distributions in the inner and $\sim r^{-2}$ profiles ($r$: distance from the core center) in the outer regions. In general these cores are at least partially shielded, i.e., the visual extinction near the boundary of the core $A_V \geq 2$ mag. It was also shown that for young low-mass cores (starless or prestellar) the temperatures of gas (Crapsi *et al*., 2007) and dust (Stutz *et al*., 2010; Launhardt *et al*., 2013) have in the inner region lower values than in the outer. The related variation range and vary between 5 and 15 K. The density profiles of the gas and dust phase correlate while the temperature profiles of both phases differ (Meng *et al*., 2013).

In contrast to the starless core, the inner region of the early protostellar core can heat up to $10^2$–$10^3$ K and is called hot corino. In the center of this hot corino a nearly hydrostatic gas sphere forms as the precursor of the protosun. The complete gravitational collapse of the cloud core proceeds relatively fast in approximately 0.5 Myr (Williams and Cieza, 2011), whereby half of the mass is accreted in less than 10% of this time period. Since the cloud core rotates, in the course of the collapse a geometrically thick disk forms with an increasing radius influenced by the rotation rate of the core and the time dependent accretion rate (Stahler *et al*., 1994). At the end of the collapsing core stage only 0.1–10% of the total stellar mass is contained in this disk. Consequently, the mean accretion rate in our SN-model must be less than $10^{-6}$ $M_O$/year. However, observations (Baraffe *et al*., 2009) have shown that the accretion rate can reach values higher than $10^{-4}$ $M_O$/year for short periods. These episodic accretion events are discussed in more detail by Stamatellos *et al*. (2012). In general, gravitational collapse simulations are performed numerically (e.g., Krumholz *et al*., 2007; Commerçon *et al*., 2008; Saigo *et al*., 2008; Schönke and Tscharnuter, 2011) or assuming that a self-similar solution (Barenblatt and Zeldovich, 1972) may exist for a special range of the collapsing core (Shu, 1977; Whitworth and Summers, 1985; Boily and Lynden-Bell, 1995: Fatuzzo *et al*., 2004). During the collapse, the spherical envelope vanishes and the vertical extension of the disk shrinks clearly.

The last stage of our SN-model, called late solar nebula, is not part of the reported study. However, the calculated abundances at the end of the major collapse phase are used as initial chemical values for the disk phase (Fig. 1). The major collapse phase has produced a massive protostar in the center of the core. Thus, our disk stage can be described by a geometrically thin but optically thick axially symmetric structure with approximately Keplerian rotation of its material (Takeuchi and Lin, 2002, 2005; Takeuchi *et al*., 2005). Both components of this material, i.e., the gas and dust phase, are partly decoupled in their dynamic and thermal evolution. Since the protostar evolves to a young highly active star in 1–3 Myr, the gas component of the disk evaporates and it becomes an optically thin disk. The dust coagulates to pebbles, which finally grow to proto-planets (Jansson and Johansen, 2014) and by stochastic accretion (Morbidelli *et al*., 2012) to planets.

We assume, that the chemical and dynamical evolution of the solar nebula proceeds according to the scheme presented in Fig. 1. This scheme reflects primarily an isolated star formation observed in Bok globules (Stutz *et al*., 2010) contrasting to clustered star formation (Battersby *et al*., 2014). One perceives, that the physical and chemical initial conditions of the collapsing cloud core and the rotating disk are determined by the processes, which govern the evolution in the quasi-stationary and in the collapsing core, respectively. In the presented study, we describe the two modules derived for the first two stages of our SN-model. The physical differences between both cloud cores require the construction of two independent modules to simulate the dynamical evolution of each core. However, in contrast to physics, the chemical processes in all three stages can be described by a single module to solve the rate equations which provide the time and radial dependent abundances of the chemical species in the gas and dust phase. In addition to

the solver of the rate equations, the module contains a database comprising parameters for about 7,000 reaction rates. Dust phase reactions, occurring on the surface of the dust grains, are important for the first stage of our SN-model (Hasegawa *et al*., 1992; Hasegawa and Herbst, 1993). Due to the cold surfaces the dust grains accrete an ice mantle composed of adsorbed species since a number of species can be formed in large abundances on cold dust grains only ($H_2O$, CO, $CH_4$, $NH_3$, etc.). The gas phase reactions and their related parameters for the reaction coefficients are taken from the OSU-astrophysical database (Smith *et al*., 2004). In addition one needs a number of parameters for dust reactions and for the transitions from gas to dust species and *vice versa*. These data, given by Semenov (2006) and Semenov and Wiebe (2011), are incorporated into the "ALCHEMIC" code, which was developed and tested by Semenov *et al*. (2010).

The observation of the starless dense cores, which can be hydrostatic or prestellar cloud cores, provides knowledge concerning the thermal and kinematic structure as well as the chemical properties of these objects (Crapsi *et al*., 2007; Maret *et al*., 2007). In a number of cases the indirect retrieval of radial gas flow signatures (asymmetry between blue- and redshifted wings in the spectral profile of optically thick emission lines such as $HCO^+$), requires an advanced observation techniques (Schnee *et al*., 2013) combined with a lot of modelling effort (Keto *et al*., 2014) to derive the putative radial profiles of the state values (density, temperature, and velocity) for prestellar cores. Currently, gravitationally bound, starless cores are considered as static, oscillating, or contracting spheroidal objects. In order to derive chemical abundances from emission lines observed in starless cores, one needs to understand the formation of these lines which depends not only on the chemical composition of the gas inside the core but also on the validity of the chosen physical core model (Keto *et al*., 2014). Recently, the water abundance of the prestellar core L1544 was derived from the observation of the absorption line formed by the ground state transition of ortho-$H_2O$ (Caselli *et al*., 2012). They have shown that the observed water amount adds up to ~$1.5 \times 10^{-6}$ $M_O$ for a radius of $10^4$ AU. Based on the Herschel observations relative $H_2O$ abundances with respect to the total hydrogen abundance (denoted by the abundance ratio $x_{H2O} = [H_2O]/([H]+2[H_2])$) were derived in the range between $10^{-10}$ and $10^{-9}$ in the gas phase. These abundances result from the non-thermal desorption of water molecules from the ice mantle around dust grains. The UV photons can be produced by the scattering of cosmic rays on $H_2$ molecules or originated from the far UV interstellar radiation field (ISRF) defined between 6 and 13.3 eV (corresponding to 91.2 and 207.0 nm). In warmer regions the water amount in the gas phase is higher because of thermal desorption. Indeed, Parise *et al*. (2005) obtained nearly $3 \times 10^{-6}$ for the relative abundance $x_{H2O}$ in the inner region of the low mass binary proto-star system IRAS 16293-2422 and $5 \times 10^{-7}$ for its outer range. Even higher abundance values of $x_{H2O} \sim 10^{-5}$–$10^{-4}$ are found for an outflowing gas towards NGC1333 (Kristensen *et al*., 2010) which are lower than the value ($x_{H2O} \sim 4 \times 10^{-4}$) retrieved from observations towards the outflow region of Orion KL using a specific model of shocked gas (Franklin *et al*., 2008). It is interesting to mention that this value is close to the one ($6.5 \times 10^{-4}$) found by Neill *et al*. (2013) for a small gas clump towards the Orion hot core. Other relative water abundances derived by Neill *et al*. (2013) for in Orion KL regions are about two magnitudes smaller and comparable with ratios obtained for the inner IRAS 16293-2422 core (Parise *et al*., 2005). A discussion about the uncertainty of the determined $x_{H2O}$ values caused by complex, model related interpretation methods of the observed data is imparted by Visser *et al*. (2013).

In addition to the relative abundance of $H_2O$ in the gas phase obtained from Herschel data, the observation of deuterated water lines towards the hot corinos of low mass proto-stars take advantage of interferometric measurements. Typical examples are the observations of the hot corinos IRAS2A and IRAS4A in NGC 1333 by Taquet *et al*. (2013) and the observation of the proto-binary IRAS 16293-2422 by Persson *et al*. (2013). They observed the deuterium content of water given by the abundance ratio of the deuterated to the non-deuterated molecules ($x_{HDO}/x_{H2O} = [HDO]/[H_2O]$) in % which is often higher than the corresponding deuterium content of the Earth ocean (156 ppm) defined by the Standard Mean Ocean Water (SMOW). Hereafter, the deviation of D/H ratio from the SMOW is given as $\delta D$ (‰) = $(0.5 \times ([HDO]/[H_2O])/(D/H)_{SMOW} - 1) \times 1000$. The ratios published by Taquet *et al*. (2013) vary for IRAS2A between 0.3% ($\delta D$ = 8,600‰) and 8% ($\delta D$ = 255,000‰) and for IRAS4A between 0.7% ($\delta D$ = 21,400‰) and 3% ($\delta D$ = 95,200‰). The observations of Persson *et al*. (2013) have given about 0.09% ($\delta D$ = 1,880‰) for a slightly better spatial resolution and a closer target. Using Herschel data Emprechtinger *et al*. (2012) have obtained an even smaller value of ~0.02% ($\delta D$ = –333‰) for the hot core NGC 6334 I towards a high-mass star forming region. Coutens *et al*. (2013) have even detected double deuterated water molecules by employing Herschel data and observing the colder envelope and the hot corino region towards IRAS 16293-2422. They obtained an abundance ratio of $D_2O/H_2O \sim 0.5\%$. However, this ratio can be derived only if one places an additional translucent cloud layer around the IRAS 16293-2422 source.

It is the goal of this study to simulate the relative abundances for $H_2O$, HDO and $D_2O$ using the first two stages of our SN-model (Fig. 1). A number of approaches to

*Table 1. Heating and cooling processes in the gas and dust phase considered in Eqs. (4) and (5) (ro-vib.: rotation-vibration)*

| Gas | | Dust | |
|---|---|---|---|
| Cooling | Heating | Cooling | Heating |
| $\Lambda_{gas}$: radiation of excited ro-vib. lines of CO, CS, HCN | $\Gamma_{cr}$: cosmic ray ionisation of H, $H_2$, He | $\Lambda_{dust}$: infrared radiation of dust grains | $\Gamma_{dust}$: absorption of UV radiation |
| $\Lambda_{gas}$: radiation of excited CO, $C^+$ and finally $H_2$ (increasing temp.) | $f_z\Gamma_{H2}$: hot $H_2$ molecules formed in the dust phase | 〃 | $\Gamma_{coll}$: collision with gas particles |
| $\Lambda_{coll}$: collision with dust grains | $\Gamma_{photo,1}$: far UV radiation causing $H_2$ dissociation | 〃 | $(1-f_z)\Gamma_{H2}$: direct absorption of energy produced by $H_2$ formation |
| $\Lambda_{photo}$: recombination of hot $e^-$ with positively charged grains | $\Gamma_{photo,2}$: hot $e^-$ from photo-ionization of C or dust | 〃 | 〃 |

model the chemical evolution of dark clouds, prestellar or protostellar cloud cores have been presented (e.g., Boland and de Jong, 1984; Ceccarelli *et al*., 1996; Bergin *et al*., 1997, 2006; Nejad and Wagenblast, 1999; Drouart *et al*., 1999; Rodgers and Charnley, 2003; Doty *et al*., 2004; Lee *et al*., 2004; Aikawa *et al*., 2005, 2008, 2012; Wakelam *et al*., 2006, 2014; Garrod and Herbst, 2006; van Weeren *et al*., 2009; Visser *et al*., 2009, 2011; Thi *et al*., 2010; Sipilä, 2012; Furuya *et al*., 2013; Yang *et al*., 2013; Garrod and Weaver, 2013; Pagani *et al*., 2013; Hincelin *et al*., 2013; Taquet *et al*., 2014; Vaytet *et al*., 2014). These models consider point, radially or axially symmetric core models combined with a more or less complex chemical database. With the models most comparable to our approach (Aikawa *et al*., 2008, 2012; Wakelam *et al*., 2014) we will later compare our results. Models which complement our study since they have tested the chemical evolution in the disk phase (Thi *et al*., 2010; Furuya *et al*., 2013) allow to estimate the evolutionary trend of the water deuteration in the late solar nebula while other models (Pagani *et al*., 2013; Taquet *et al*., 2014) report on a chemical network considering not only the deuterium chemistry but also the influence of the two spin-energetic states of the hydrogen molecule. The latter have identified an important source of reducing the deuteration of water, the ortho hydrogen molecules and their ions. Finally, Vaytet *et al*. (2014) has studied the energetic influence of the ortho hydrogen molecule on the equation of state of the gas-dust mixture and, thus, the interaction between the chemical and hydrodynamic evolution of the cloud core.

Our model uses a cold, radially symmetric core as initial state for the formation of our sun with a fixed but arbitrary life time between 1 and 6 Myr. In order to provide a relatively self-contained presentation of our SN-model, in the next section we expound briefly the main aspects of the evolving cloud core without going into too much mathematical detail. These details are explained in Tornow *et al*. (2014a) for the quasi-stationary core, while for the collapsing core, they can be found in Tornow *et al*. (2014b). The third section presents and explains the simulated water abundances and deuterium fractionation. Finally, we discuss the results and give a short outlook concerning open problems.

## Model Description

*The quasi-stationary core*

We assume that our Sun has formed as a relatively isolated star from a cloud core with a mass of about 1 $M_O$ and isotropic boundary conditions. Our quasi-stationary core model can be understood as a gas-dust sphere with radially symmetric gas temperature and density profile. The dominance of the gas with respect to dust results from the canonical dust to gas mass ratio given by 0.01. Further, the core is assumed to be located in a region with a low ISRF, whose intensity scaling amounts to maximally 3 Habing (1 Habing = $1.2 \times 10^{-4}$ erg/cm$^2$/s/sr; Tielens, 2005). The sphere is partially shielded from this field by thin inter-core material ($A_V = 2$), which corresponds to a radially symmetric gas shell having a constant gas density. The radial profiles of gas mass, $M$, gas density, $\rho$, gas pressure, $P$, and gas temperature, $T$, are computed from the Poisson and the momentum conservation equations as well as from the ideal gas equation

$$\frac{\partial M}{\partial r} = 4\pi r^2 \rho \tag{1}$$

$$\frac{\partial P}{\partial r} = -\rho \frac{GM}{r^2} \tag{2}$$

$$P = \frac{k_B}{m_p} \rho T = n k_B T \tag{3}$$

with the gravitational constant, $G$, the Boltzmann constant, $k_B$, the gas particle mass, $m_p$, and the radius, $r \in [0, R_C]$. The boundary conditions follow from core mass $M_O = M(R_C)$, shell density $\rho_0 = \text{const.} = \rho(R_C)$ and tempera-

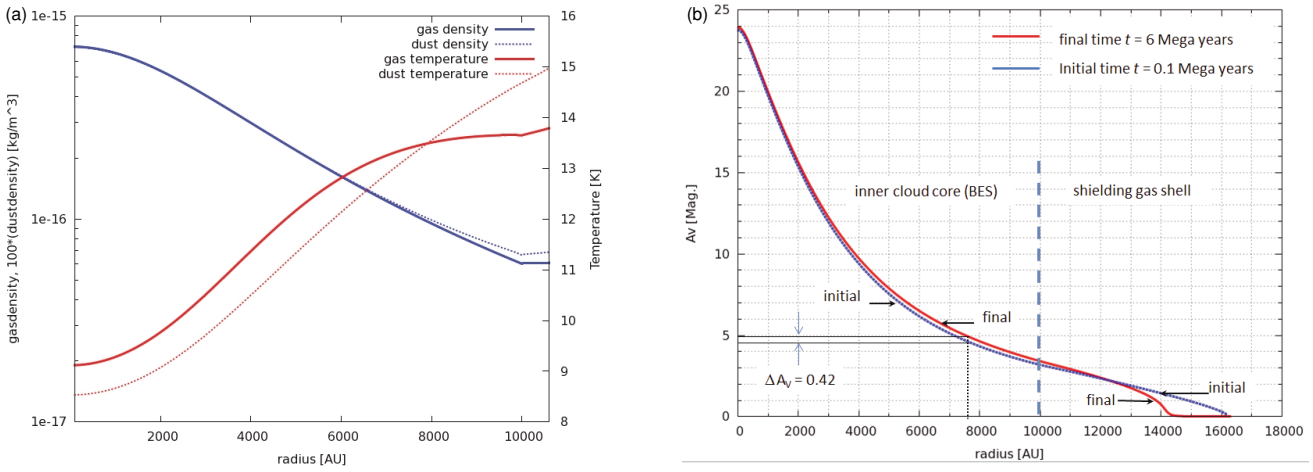


*Fig. 2. (a) Gas and dust profiles (ascending temperatures and descending densities) of the core for the dust size distribution of Mathis et al. (1977) obtained after about 6 Mega years. The dust density is multiplied with 100. The boundary of the inner sphere is located at ~$10^4$ AU (figure taken from Tornow et al., 2014a). (b) Initial and final profile of visible extinction of the dust, $A_V$, depending on the profile of the column density and the size distribution of Mathis et al. (1977). The symbol $\Delta A_V$ is defined as $\Delta A_V = max_{r<RC}\,(A_V\,(t = 0.1$ Mega years$) - A_V\,(t = 6$ Mega years$))$.*

ture $T_0 = T(R_C)$. Since the gas of the central core is nearly molecular, the averaged mass of one gas particle can be written as $m_p = \mu_p m_H$, with the mass of a hydrogen atom $m_H$, $\mu_p = 2.34$ and the particle number density is given by $n = \rho/m_p$. A mass factor $\mu_p$ of 2.34 arises, since in addition to hydrogen molecules, the gas consists of a small mass fraction of helium and traces of so called metals (e.g., oxygen, carbon, iron). Two further equations are needed to determine the profiles of gas and dust temperature. They follow from the thermal balance between the cooling and heating processes which couple both phases to each other. Thus, we obtain for the gas phase

$$\Gamma_{cr} - \Lambda_{gas} + \Gamma_{photo} - \Lambda_{photo} + f_z \Gamma_{H2} - g_{coll}\left(T - T_d\right) = 0 \quad (4)$$

and equivalently for the dust phase

$$\Gamma_{dust} + \left(1 - f_z\right)\Gamma_{H_2} - \Lambda_{dust} + g_{coll}\left(T - T_d\right) = 0 \quad (5)$$

with the dust temperature, $T_d$. Equations (4) and (5) depend also on the dust density, $\rho_d$, and are valid at each radial grid point of the core and the shell. The meaning of the various parameters in the balance equations, explained in Table 1, are explicitly given in Tornow *et al.* (2014a).

To calculate the difference $\Gamma_{dust} - \Lambda_{dust}$ in Eq. (5), we employ the dust size distribution of Mathis *et al.* (1977) and the method of Zucconi *et al.* (2001) to solve the radiative transfer equation. Other size distributions (e.g., Zubko *et al.*, 2004) cause deviations of <3% along the profile of the relative water abundance calculated from our SN-model (Tornow *et al.*, 2014a). Since the coagulation of dust grains is less important for the early solar nebula, the chosen size distribution can be kept constant. However, the dust to gas mass ratio changes due to the motion of grains, which is caused by the radiation pressure of the surrounding ISRF. The grain velocity, $\upsilon_{d,\bar{a}}$, depending on the grain size $a$, results from the conservation equation of the dust momentum (Whitworth and Bate, 2002). In order to save the computation power, we consider the mean grain size, $\bar{a}$, averaged for the chosen size distribution. Since the velocity, $\upsilon_{d,\bar{a}}$ is small, the momentum conservation can be written as a simple force balance

$$m_{d,\bar{a}} \ddot{r}_{d,\bar{a}}(t) = D_{\bar{a}}\left(\rho, \rho_{d,\bar{a}}\right) - \pi \bar{a}^2 \psi\left(\rho_{d,\bar{a}}\right) P_{ISRF}$$
$$\text{with } r_{d,\bar{a}}(0) = \dot{r}_{d,\bar{a}}(0) = 0 \quad (6a)$$

where $m_{d,\bar{a}}$ is the dust mass of a single grain, $\rho_{d,\bar{a}}$ is the dust density, $D_{\bar{a}}$ is the deceleration of the grains because of the gas drag, $\psi$ is the attenuation of the radiation field, $P_{ISRF}$ is its radiation pressure, and $r_{d,\bar{a}}(t)$ is the time dependent shift of the grain according to its initial position. Knowing the grain velocity, $\upsilon_{d,\bar{a}} = \dot{r}_{d,\bar{a}}(t)$ one can find the dust density, $\rho_{d,\bar{a}}$, by solving the continuity equation

$$\frac{\partial M_{d,\bar{a}}}{\partial t} = -4\pi r^2 \rho_{d,\bar{a}} \upsilon_{d,\bar{a}} \quad \text{with} \quad \frac{\partial M_{d,\bar{a}}}{\partial r} = 4\pi r^2 \rho_{d,\bar{a}}. \quad (6b)$$

One can assume, that the grain velocity and density change

*Table 2. Specification of the density function in each zone i, i = 1, 4*

| $\rho_1(r, t)$ | $\rho_2(r, t)$ | $\rho_3(r, t)$ | $\rho_4(r, t)$ |
|---|---|---|---|
| $\frac{\rho_{01}}{1+(r/a_1)^{\gamma_1}}$ | $\frac{\rho_{02}}{1+(r/a_2)^{\gamma_2}}\left[\frac{\omega_1}{r}\right]^{\chi_2}$ | $\rho_{03}\left[\frac{\omega_2}{r}\right]^{\chi_3}$ | $\rho_{04}\left[\frac{\omega_3}{r}\right]^{\chi_4}\cos^2\left(\frac{\pi r}{2R_c}\right)+\overline{\rho}$ |

only slowly with time. In order to solve Eqs. (1) to (6) we used an iterative method (Kupper, 2014), in which one inserts $\rho_{d,\bar{a}}$ into Eqs. (4), (5), and (6a).

The temperature profiles of the gas and dust as well as the gas density profile are derived considering (1), (2) and (3). These data are then used to find the new profile of the dust density from Eq. (6b) and the next iteration step follows. The complete iteration procedure converges very fast to stable solutions. In Fig. 2a, the final results of these profiles are presented. The density profile corresponds to the Bonnor-Ebert sphere (BES) described by Bonnor (1956) and Ebert (1957). This sphere has a clearly defined radius, a final mass, and a regular density solution.

Due to Eqs. (4) and (5) one obtains different radial profiles for the temperatures of the gas and dust phase (see Fig. 2), where the first profile varies between 9 and 13.7 K and the latter varies between 8.5 and nearly 15 K. Compared to the results published by Bergin *et al.* (2006) for the B 68 core the dust temperature is 1–2 K lower, but they have considered a lower far UV radiation intensity (0.2 Habing).

Figure 2b shows the initial and final profiles of the visible extinction $A_V$. Since the core is only partially shielded, the photo-chemistry has a significant effect on the radial profile of the relative water abundance. In addition to the intensity of the ISRF, the rates of the photo-reactions depend also on the visual extinction $A_V$. Even if the difference between both profiles is fairly small ($\Delta A_V \sim 0.42$), the chemical abundance of $H_2O$ or other molecules is also influenced.

*The collapsing cloud core*

In order to obtain a collapse model for the core with an arbitrarily high spatial resolution the magnetohydrodynamic (MHD) equations of a partially ionized gas are solved with a semi-analytical approach. The related MHD equations are the Poisson, continuity, momentum, and induction equation with the following expressions:

$$\frac{\partial M}{\partial r} = 4\pi r^2 \rho \text{ with } \frac{\partial \Xi}{\partial r} = \frac{GM}{r^2} \tag{7}$$

$$\frac{\partial M}{\partial t} = -4\pi r^2 \rho u \text{ or } \frac{\partial \rho}{\partial t} + \frac{1}{r^2}\frac{\partial}{\partial r}\left(r^2 \rho u\right) = 0 \tag{8}$$

$$\rho\frac{\partial u}{\partial t} + \rho u\frac{\partial u}{\partial r} = -\frac{\partial}{\partial r}\left(P + \frac{b^2}{2\mu_0}\right) - \frac{b^2}{\mu_0 r} - \rho\frac{GM}{r^2} + \tau_{VC} f$$
$$\text{with } f = \frac{2}{3}\left(2\left(\frac{\partial^2 u}{\partial r^2} + \frac{2}{r}\frac{\partial u}{\partial r}\right) - \frac{u}{r^2}\right) \tag{9}$$

$$\frac{\partial b}{\partial t} + \frac{1}{r}\frac{\partial}{\partial r}(rbu) = \frac{\eta}{r^2}\frac{\partial}{\partial r}\left(r^2\frac{\partial b}{\partial r}\right). \tag{10}$$

Due to the radial symmetry the radius, $r \in [0, R_C]$ and the time, $t \in [0, T]$ are the independent variables and $u$ and $b$ denote the gas velocity and the toroidal magnetic field of the collapsing core. $R_C$ and $T$ symbolize the size of the core and the collapse duration, respectively. A fitting relation which expresses the resistivity, $\eta$ as function of the gas temperature and the ionisation degree of the gas (actually one has to call it plasma) can be find in Machida *et al.* (2007) or in appendix of Tornow *et al.* (2014b). The gas to dust mass ratio, kept fixed during the collapse, corresponds to the one of a 6 Myr old quasi-stationary core (Fig. 2). Further, we used the equation of state (EOS) given by

$$P = K_P \rho^s. \tag{11}$$

The parameters $K_P$ and $s$ depend on the time and $s$ corresponds to the ratio of the specific heat coefficients. Consequently, the conservation of energy

$$w_H = \frac{j^2}{\sigma} + \rho\hat{h} + \frac{1}{r^2}\frac{\partial}{\partial r}\left(r^2\kappa\frac{\partial T}{\partial r}\right) + \rho Q = 0$$
$$\text{with } \hat{h} = 2\tau_{VC}\rho\left(\frac{\partial u}{\partial r}\right)^2 - \frac{2}{3}\rho\tau_{VC}\left(\frac{1}{r^2}\frac{\partial}{\partial r}\left(r^2 u\right)\right)^2$$
$$\text{and } j = -\frac{1}{r}\frac{\partial}{\partial r}\left(\frac{rb}{\mu_b}\right),\ \mu_b = 4\pi\times 10^{-7}\ \text{Vs/Am} \tag{12}$$

must be fulfilled. The total heat rate $w_H$ consists of Julian and frictional heat rates, the heat transport in the core according to heat conductivity $\kappa(\rho, T)$ and the sum $Q = \Gamma - \Lambda$ of energy loss and gain per unit time. Since the rota-

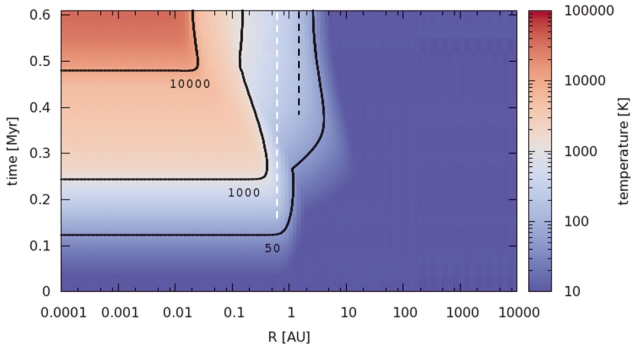


*Fig. 3. The evolution of the gas temperature on an Eulerian grid. The white dashed line indicates the temperature required for hot neutral reactions, and the black dashed line indicates the thermal desorption temperature for $H_2O$ (figure taken from Tornow et al., 2014b).*

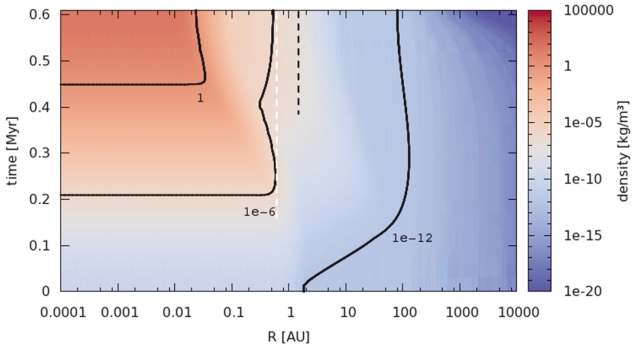


*Fig. 4. The evolution of the gas density on an Eulerian grid. Note the nonlinear correlation between ρ and T, which slightly changes the spatial appearance of the hot corino (figure taken from Tornow et al., 2014b). The white and black dashed lines are the same as those in Fig. 3.*

tion of the core is not considered in our study, a specific definition for the viscosity parameter $\tau_{VC}$ is chosen: $\tau_{VC} = k_\tau c_s R_C$ (Regev and Shaviv, 1981). The tuning value, $k_\tau$, depending on Reynolds number, $Re$, and sound speed, $c_s$, is given by

$$k_\tau = \left(\langle u \rangle / c_s\right) Re^{-1}. \tag{13}$$

Note, that the ratio $(k_B T)/(\mu_p m_H)$ gives the quadratic sound speed. Now, the following analytical expression for the gas density $\rho$ is introduced into the MHD equations (7) and (8)

$$\rho(r,t) = \begin{cases} \rho_1(r,t) & \text{if} \quad 0 \le r < \omega_1(t \le T) \\ \rho_2(r,t) & \text{if} \quad \omega_1(t \le T) \le r < \omega_2(t \le T) \\ \rho_3(r,t) & \text{if} \quad \omega_2(t \le T) \le r < \omega_3(t \le T) \\ \rho_4(r,t) & \text{if} \quad \omega_3(t \le T) \le r < R_C \end{cases} \tag{14}$$

where the densities in the radial intervals are given in Table 2. The average velocity, $\langle u \rangle$ in Eq. (13) is computed for each of these radial intervals and the unknown coefficients $a_i$, $\omega_i$, $\gamma_i$, $\chi_i$, and $\rho_{0i}$ correspond to 14 time-dependent functions. The resulting complete solution of the MHD equations is explained in Tornow *et al.* (2014b).

In this study the chemical processes are the main topic, but the consequential distributions of the state variables for our collapsing core model will be shown to simplify the understanding of the obtained results from the chemical simulations. According to Ceccarelli (2004), a hot corino is a region located close to the center of the collapsing cloud core, clearly smaller than 150 AU in a low-mass star forming target.

It seems necessary to note, that a determination of the

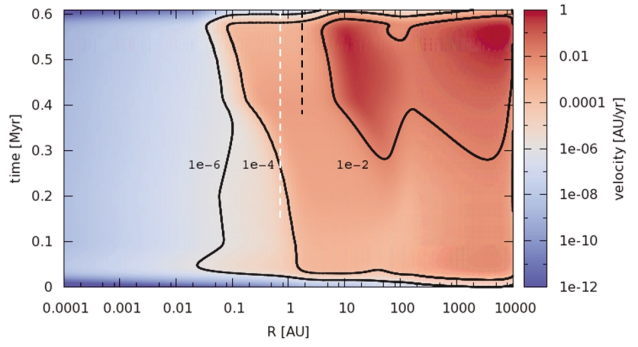


*Fig. 5. The evolution of the gas velocity on an Eulerian grid. We have an outside-in collapse in contrast to Shu (1977), but similar to Larson (1969), Penston (1969) and Gong and Ostriker (2009). Note, $c_s$ = 0.038 AU/yr at T = 10 K (figure taken from Tornow et al., 2014b). The white and black dashed lines are the same as those in Fig. 3.*

outer boundary of the hot corino from observations is hard to achieve (Maret *et al.*, 2004; Jørgensen and van Dishoeck, 2010). In particular the source IRAS16293-2422 identified as binary proto-stars has a large hot corino range $R_{100K}$ = 133 AU (with $R_{100K}$ outer boundary with $T$ = 100 K). In contrast to the binary source, there is the "lukewarm hot corino" L1527 (IRAS 04368+2557) which has a much smaller value for $R_{100K}$ = 20 AU (Hassel *et al.*, 2008). However, according to Tobin *et al.* (2013), this object has a turbulent disk with a radius of 125 AU related to our optically thick disk stage (Fig. 1).

Figures 3, 4, and 5 illustrate the evolution of the gas temperature, density, and velocity on an Eulerian grid. One recognizes in Fig. 3, that the distribution of the temperature corresponds to an isothermal process in a large temporal and radial range. Accordingly, we call our model

*Table 3. Initial abundances for the species (X) relative to the molecular and atomic hydrogen abundance given as 12 + log(x) with $x_X = X/(H + 2H_2)$ for the quasi-stationary cloud core (Wakelam et al., 2006; Kupper, 2014) and solar photosphere (Lodders et al., 2009)*

| Species $X$ | Cloud core | Solar photosphere | Element | Cloud core | Solar photosphere |
|---|---|---|---|---|---|
| $H_2$ | 11.70 | — | HD | 7.18 | — |
| He | 10.99 | 10.925 | $S^+$ | 4.96 | 7.14 |
| H | 9.30 | — | $Fe^+$ | 3.44 | 7.45 |
| O | 8.26 | 8.73 | $Mg^+$ | 4.04 | 7.54 |
| $C^+$ | 7.90 | 8.39 | $Na^+$ | 3.35 | 6.30 |
| N | 7.39 | 7.86 | $Si^+$ | 3.99 | 7.52 |

a cold collapse. The formation of the hot corino starts at ~0.13 Myr with $s \sim 4/3$ (see Eq. (11)). The temperatures are at least high enough to allow water desorption from the dust phase. The hot corino becomes a shell as soon as its central temperature is high enough to form a collisional hydrogen dissociation front ($T \sim 2{,}000$ K). Behind this front a hydrostatic source evolves by accreting matter from outwards. Its temperature increases slowly (due to a proceeding $H_2$ dissociation which requires 4.48 eV per molecule while the mean available thermal energy in the hot corino is only ~0.74 eV, Stahler and Pallas, 2004) and rises afterwards if all species are atomic. Hydrogen ionization starts and the protostellar source forms.

In Fig. 4 the iso-line $\rho_{\rm inn} = 1$ kg/m$^3$ (nearly air density) indicates the inner boundary of the hot corino while the outer boundary is located between the iso-lines $\rho_{\rm o1} = 10^{-6}$ kg/m$^3$ and $\rho_{\rm o2} = 10^{-12}$ kg/m$^3$. (Masunaga *et al.*, 1998; Masunaga and Inutsuka, 2000). Compared with Fig. 3, the related temperatures at the iso-lines suggests that a typical adiabatic relation as given by Saigo *et al.* (2008) would produce a nearly ten-fold higher temperature in this range, i.e., our approach of a multi-zone density (see Eq. (14) and Table 2) includes a solution with a temperature-density relation that describes a gas-dust mixture for the collapsing material with excellent cooling properties. A further consequence of the approach is the slow gas infall into the inner core center (Fig. 5).

Indeed, at the early collapse period and between the center and 10 AU in the later one recognizes a flat gradient of sub-sonic velocities. For the late outer collapse region this gradient becomes steeper and the velocities super-sonic. The numerical codes of Schönke and Tscharnuter (2011) as well as Saigo *et al.* (2008) produce higher inflow velocities in the inner range. The former employed an energy conservation equation including radiation instead of the adiabatic density-temperature relation and derived even higher values in the outer core regions. However, if one compares our densities with the radial dependency of the density distributions, which they have obtained, they agree well with each other.

*The chemical model of the gas and dust phase*

*General aspects* The gas phase of our chemical model is based on the Nahoon model of Wakelam *et al.* (2006), while the dust phase reactions are taken from the Heidelberger "ALCHEMIC" code developed by Semenov and Wiebe (2011). In both stages of our SN-model all chemical abundances have been simulated with rate equations (Herbst and Klemperer, 1973; Prasad and Huntress, 1980; Langer and Graedel, 1989; Lee *et al.*, 1996; Aikawa *et al.*, 2008). If $k$ denotes the species number with $N = \max(k)$, the relative abundances are defined by

$$x_k = \frac{\rho_k}{\rho} = \frac{n_k}{n} \quad \text{with} \quad \rho = \sum_{k=1}^{N} \rho_k$$

where the latter equality follows because of the introduction of an averaged particle mass $m_{\rm p}$. For some $k_0$, one has $x_{k0} \equiv x_{\rm H2O}$ and $n_{k0} = n_{\rm H2O} = H_2O$ if one assumes that $\rho \approx \rho_{\rm H} + 2\rho_{\rm H2}$, i.e., if one adds molecular and atomic hydrogen together, they are the dominant species. This is true for all non-ionized interstellar clouds keeping in mind that the second most frequent element in the universe, He, is chemically inert and considered by its mass only. All species in the medium have the same streaming velocity which is set to $u = 0$ for the quasi-stationary core and $u = \upsilon_{\rm r}$ (Fig. 5) for the radial inflow velocity of the collapsing core. Thus, the rate equations, corresponding to $N$ continuity equations (second form of Eq. (8) in the previous section), can be written as

$$\frac{\partial x_k}{\partial t} + u\frac{\partial x_k}{\partial r} = \hat{\Gamma}_k - \hat{\Lambda}_k \qquad (15)$$

where the symbols $\Gamma_k$ and $\Lambda_k$ contain all the formation and destruction processes for species $k$, respectively. Since the number of chemical species is very large, one should avoid solving thousands of coupled partial differential equations by simulating the chemical evolution of all species in the Lagrange frame (Lufkin and Hawley, 1993),

which can be seen as a large bundle of paths oriented from the outer core boundary to the center. Then, the chemical evolution of an arbitrary gas pocket can be calculated along this path leading to a simplified version of Eq. (15). If we split the set $\{x_k\}_{k=1,N}$ into two subsets, one for the dust phase and one for the gas phase: $x_k \rightarrow (x_p, x_q^*)$, one obtains the two sets of differential equations

$$\frac{dx_p}{dt} = \hat{\Gamma}_p - \hat{\Lambda}_p, \quad \frac{dx_q^*}{dt} = \hat{\Gamma}_q^* - \hat{\Lambda}_q^* \quad \text{with} \quad p = 1, N_p, \quad q = 1, N_q \tag{16}$$

with the condition $N_p + N_q = N$. Other conditions are of course mass and charge conservation. Both systems differ chemically but they are coupled to each other since the formation and destruction functions $\hat{\Gamma}_p$, $\hat{\Lambda}_p$, $\hat{\Gamma}_q^*$ and $\hat{\Lambda}_q^*$ depend on the relative abundances $(x_{p'}, x_{q'}^*)$ and lead to an interaction between both phases. Numerically, both sets of the differential equation (16) are solved simultaneously and treated as one.

The initial abundances needed to solve the differential equation are given in Table 3. We use the KIDA database (http://kida.obs.u-bordeaux1.fr/models/kida.uva.2011.zip) which is related to the former OSU (Ohio State University) database, in order to simulate the reactions of 474 gas species and compute their corresponding coefficients (Wakelam *et al*., 2006, 2010, 2012) as well as to simulate the hot core or hot corino chemistry (http://kida.obs.u-bordeaux1.fr/models/osu_HighT.zip). The data to calculate dust surface reactions, which are desorption energies from these surfaces and the energetic potential barriers between grain sites (to compute the hopping or tunneling rates) on these surfaces, can be taken from the ALCHEMIC database of Semenov (2006) and Semenov *et al*. (2010) for about 200 dust species. A parser program was developed, which reads the described databases and constructs the temperature related system of coupled differential see above (16). In order to calculate the chemical abundances, we employed the DLSODES solver of the odepack (http://www.netlib.org/odepack/) (Brown and Hindmarsh, 1989), which iteratively solves the differential system for the species of the gas and dust phase simultaneously. Now the chemical reactions for all elements in Table 3 except for HD can be considered.

Further technical details concerning the simulation of the chemical reactions are discussed in Semenov (2006) and Kupper (2014). Especially the calculation of the formation and destruction function for the chemical species $(x_{p'}, x_{q'}^*)$ is explained there. Of course, our chemical simulation depends on the initial chemical conditions for the quasi-stationary core which are given in Table 3 while the chemical abundances obtained from this core after 6 Myr of evolution are the chemical input data of our collapsing core (see Fig. 1). Comparing the initial element abundances of the cloud core with the abundances of the solar photosphere given by Lodders *et al*. (2009), one recognizes that the gas in the cloud core is depleted of heavy elements, such as Si, Mg, Na, and Fe but also lighter ones such as C, O, and S. Both groups are refractory solid forming elements that produce for instance minerals or carbon clusters and are incorporated into dust grains. The temperature of the solar nebula (Fig. 3) is higher than the condensation temperatures of many minerals near the protostar ($T > 1680$ K, Lodders, 2003) and the grains vaporize quickly and transit from the solid to the gas phase. The C/O ratio, influencing the mineral building chemistry as well as the composition of ice mantles formed on dust grains, is 0.44 for the core and 0.46 for the solar photosphere, telling that our core model is slightly richer in oxygen compared to carbon.

The initial abundance distribution in Table 3 considers $H_2$, but neglects that the nuclear spin of the molecule gives rise to emergence of two isomers, denoted as ortho- and para-$H_2$. In general one considers a mixture of ortho- and para-$H_2$ whereby the ortho-isomer corresponds to a triplet quantum state with proton spins aligned parallel and the para-isomer is related to a singlet quantum state with proton spins aligned anti-parallel. In local thermal equilibrium the ortho-to-para ratio (OPR) for $H_2$ is calculated from the quotient of the corresponding rotational partition functions Gavilan *et al*. (2012). The equilibrium values for $H_2$ at 10 K is given by $OPR_{10K} \sim 4 \times 10^{-7}$. However, the indirect measurements of this ratio reported in the literature for cold cloud cores differ clearly from $OPR_{10K}$. According to Pagani *et al*. (2013) and Troscomp *et al*. (2009), it follows: $0.1 < OPR < 1$. The OPRs derived from $H_2O$ observations in the coma of comets are even larger and vary mainly between 2.5 and 3 (Dello Russo *et al*., 2005; Bonev *et al*., 2007, 2013). In addition, there are experiments investigating the OPR resulting from hydrogen molecules formed on porous amorphous water ice (Gavilan *et al*., 2012). The measurements provide an OPR of 2.91 with a large uncertainty. Overall, these data suggest a relatively high abundance of ortho-$H_2$ (compared to the equilibrium abundance) in the gas and dust (ice) phase of cold cores. However, since our chemical network is very complex and, in the collapsing core stage, the density and temperature gradients are very large, we have to perform an appropriate decrease of the number of species before adding ortho-$H_2$ to it. If the simplified network provides nearly the same results as those obtained in the presented study we have a network designed for water. Perhaps, a similar procedure can be done for other species or a small set of them. However, at the end of the next section we will come back again to the influence of a relatively large OPR.

*Aspects of $H_2O$, HDO and $D_2O$ formation* In addition to the water abundance the deuterium to hydrogen ratio (D/H) is an interesting parameter which contains information on the thermal conditions of the gas-dust material in which the water has been formed (Cazaux *et al*., 2011). Since it is the goal of this study to determine the evolution of the water abundance and the D/H of water in the gas and dust phase during the early stages of the solar nebula, we will explain the formation of water in more detail. First, the system of differential equations needs to be extended by including all the deuterium bearing species. To achieve this purpose, we applied the method proposed by Albertsson *et al*. (2013) but also used the published reactions (Brown and Rice, 1986a, b; Flower *et al*., 2004; Hiraoka *et al*., 2005; Howe and Millar, 1993; Howe *et al*., 1994; Millar *et al*., 1989; Osamura *et al*., 2005; Roueff *et al*., 2007; Tielens, 1983; Walmsley *et al*., 2004; Willacy, 2007). This way, the species number increases to about 1,900 and the number of reactions increase to about 17,330 for both phases. The energy barrier of thermal surface desorption differs with mass (Kristensen *et al*., 2011). We have chosen a factor of 1, 1.003 and 1.039 based on the mass of $H_2$, HD, and $D_2$ (Kupper, 2014).

$H_2O$ is formed in the gas phase by hot neutral reactions (Charnley, 1997), which become possible because of the increasing temperature due to the gravitational compression of the core. Typical reactions are

$$\begin{array}{lll} H_2 + O & HD + O & D_2 + OD \\ \rightarrow OH + H & \rightarrow OD + H & \rightarrow D_2O + D \\ H_2 + OH & HD + O & HD + OD \\ \rightarrow H_2O + H & \rightarrow HDO + H & \rightarrow D_2O + H. \end{array} \quad (17)$$

The neutral reactions require at least temperatures between 160–230 K to proceed efficiently and surmount the activation energy barrier (Ceccarelli *et al*., 1996; Charnley, 1997). In the cold cloud core, i.e., for temperatures lower than 20 K, large abundances of H, D, O, OH, and OD species are adsorbed on the surface of dust grains and, due to the high mobility of H and D on these surfaces (Matar *et al*., 2008), $H_2O$, HDO, and $D_2O$ are produced by surface reactions (Dulieu *et al*., 2010). In particular, a few of them (last two columns below) are emphasized theoretically by Tielens (1983), and theoretically and in the laboratory by Mokrane *et al*. (2009) and Chaabouni *et al*. (2012).

A deuterium enrichment of the water ice mantle is

$$\begin{array}{lll} H + O \rightarrow OH & O_2 + D \rightarrow O_2D & OD + D \rightarrow D_2O \\ H + OH \rightarrow H_2O & O_3 + D \rightarrow OD + O_2 & OD + H \rightarrow HDO \\ & O_2D + D \rightarrow 2OD & H_2O + D_2O \rightarrow 2HDO. \end{array} \quad (18)$$

caused by the higher sticking probability of small deuterated species (Matar *et al*., 2010). In addition, during the sublimation a sudden H-D exchange reaction is activated leading to the process $H_2O \rightarrow HDO$ (Matar *et al*., 2008). However, so far one has not observed clear evidence for a favored formation of single HD or OD species compared to $H_2$ or OH (Hama *et al*., 2012). In the gas phase of cold cores the direct formation of water molecules is less effective. Accordingly, $H_2O$ molecules and the deuterated compounds formed on the grain surface can be desorbed non-thermally via the influence of cosmic rays and far UV photons. At the end of our cold collapse the dust temperature in the hot corino region is high enough for a thermal desorption of the water molecules from the grain surfaces without changing the high D/H ratio of these molecules. A reduction of the high D/H ratio would occur, however, if UV radiation and X-rays lead to the dissociation of $H_2O$, HDO, and $D_2O$ combined with a reformation of these molecules by the already mentioned hot neutral reactions in the gas phase. This process starts as soon as the proto-star enters its T-Tauri phase while being surrounded by a solar nebula arranged in a stationary optically thick disk (compare Fig. 1). In cold cores the amount of ions is fairly low causing a low rate of ion-molecule reactions. In the outer translucent region of the core the gas phase water not adsorbed on dust grains is dissociated by the far UV radiation. The typical ion reactions which form water and its deuterated compounds are already proposed by Glassgold and Langer (1976).

$$\begin{array}{lll} H_3^+ + O & H_2D^+ + O & OD^+ + 2HD \\ \rightarrow OH^+ + H_2 & \rightarrow OD^+ + H_2 & \rightarrow HD_2O^+ + HD \\ OH^+ + 2H_2 & OD^+ + 2H_2 & \\ \rightarrow H_3O^+ + 2H & \rightarrow H_2DO^+ + 2H & \\ H_3O^+ + e & H_2DO^+ + e & HD_2O^+ + e \\ \rightarrow H_2O + H & \rightarrow HDO + H & \rightarrow D_2O + H. \end{array} \quad (19)$$

The reactions in the first and second line are characterized by charge transfer and the ones in the last line are called dissociative recombination (Larsson *et al*., 2012). These reactions occur in diffuse ($0.1 < A_V \leq 1$), translucent ($1 < A_V < 5$) but also in dark ($5 \leq A_V$) clouds which belong to the cold neutral matter phase of the interstellar medium (Turner, 1993, 2000; Hollenbach *et al*., 2012). In these dark clouds having a complete UV shielding the relative abundances of water with respect to hydrogen is less than $10^{-8}$ (Bergin and Snell, 2002) which is in agreement with the data mentioned in the Introduction and in

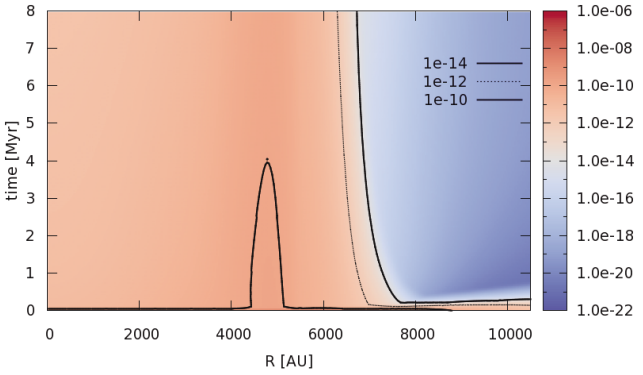


*Fig. 6. Radial and temporal distribution of the $H_2O$ abundance in the gas phase $x_{H2O}$. The patterns of the HDO and $D_2O$ abundance distributions are quite similar to the one of $H_2O$.*

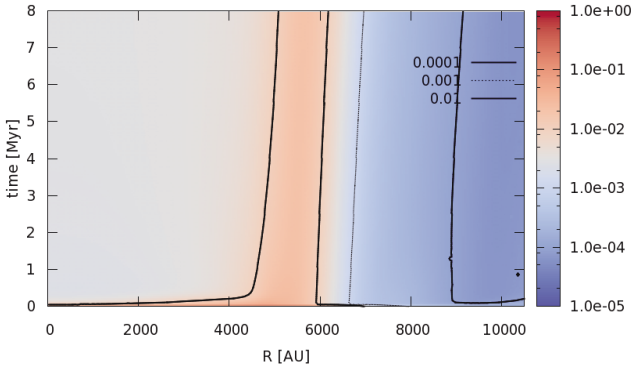


*Fig. 7. Radial and temporal distribution of the abundance ratio $x_{HDO}/x_{H2O}$ in the gas phase. The percentage variation of the abundance ratio between 0.01 and 1% corresponds to a deuterium enrichment $\delta D$ between –680 and ~+31,000‰.*

agreement with the resulting ionization fraction which is typically ~$10^{-8}$ (de Boisanger *et al.*, 1996). Deuterium fractionation can be understood by considering the exothermal reaction $H_3^+ + HD \leftrightarrow H_2D^+ + H_2$ which has a difference in the bond dissociation energy equivalent to 232 K (Roueff *et al.*, 2007). Thus, in cold dense cores the right arrow is favored leading to an enhancement of the ratio $H_2D^+/H_3^+$ with respect to the $HD/H_2$ abundance. However, this is the point to mention the OPR again. For the gas phase species $H_2D^+$ in Eq. (19) and an OPR >> 0, the following reactions (among many others) must be added to the chemical network

$$\begin{aligned} & \rightarrow \text{p-}H_3^+ + HD && \text{with } 7.7\times10^{-11} \\ & \rightarrow \text{o-}H_3^+ + HD && \text{with } 8.3\times10^{-11} \\ \text{o-}H_2D^+ + \text{o-}H_2 \; & \rightarrow \text{p-}H_2D^+ + \text{p-}H_2 && \text{with } 9.2\times10^{-11} \\ & \rightarrow \text{p-}H_2D^+ + \text{o-}H_2 && \text{with } 1.8\times10^{-10} \\ & \rightarrow \text{o-}H_2D^+ + \text{p-}H_2 && \text{with } 2.35\times10^{-10}. \end{aligned} \qquad (19')$$

Comparing the Langevin reaction rates in Eq. (19′) the first two relations are less important than the other ones but can cause a de-deuteration of the gas species (Flower *et al.*, 2006). The influence of three initial OPR values ($10^{-4}$, $10^{-2}$ and 3) of $H_2$ on the D/H ratio of water and other species observed in the coma of comets or in the interstellar ice was studied very recently by Taquet *et al.* (2014) using a semi-empirical model of a collapsing cloud core and a well-elaborated chemical network. For the maximum increase of OPR by a factor of $3 \times 10^4$, they found a small decrease of the D/H for water in the gas phase (a factor of ~2.25) and a large decrease for the ice phase (a factor of 27.2). We will keep this result in mind and will use it for our conclusions.

## Results

In Subsection "The chemical model of the gas and dust phase" we have sketched how to compute the chemical interaction between the gas and the dust phase. Here, we will also use primarily the notation *ice phase*. In our case the species of the ice phase are the same as the species of the dust phase, since in contrast to the dust mantle its nucleus does not change chemically in our model. However, this is not always the case. Water formed by hot neutral reactions could be chemisorbed by fractal dust grains in large abundances in a temperature range around 900 K (King *et al.*, 2010).

### *Formation of $H_2O$ and isotopologues in the quasi-stationary core*

We have to underline that the chemical evolution of the partially shielded core is studied, but not the one of the gas shell. Otherwise, we would have to apply special techniques developed for the photon-dominated regions, which are explained and discussed by Hollenbach and Tielens (1999).

From the simulated chemical data set for each grid point of the core, we obtain the relative gas phase abundances of $H_2O$ and its isotopologues $x_{H2O}$, $x_{HDO}$, and $x_{D2O}$ as well as the corresponding relative abundances for the ice species $x^*_{H2O}$, $x^*_{HDO}$, and $x^*_{D2O}$, which are presented and discussed in the following. According to our results, the ice mantle forms in $10^4$–$10^5$ years on the dust grains of the quasi-stationary core and changes slowly afterwards. The most frequent ice species are $H_2O$ and CO, but due to the composition in Table 3 $H_2O$ is the dominant one, i.e., $x^*_{CO}/x^*_{H2O} \leq 0.13$. A general comparison between gas and ice phase shows that the maximum abundance $x_{H2O}$ in the gas phase is nearly $10^{-10}$ (Fig. 6) and much lower than $x^*_{H2O} = 1.7 \times 10^{-4}$ (Fig. 8). The abun-

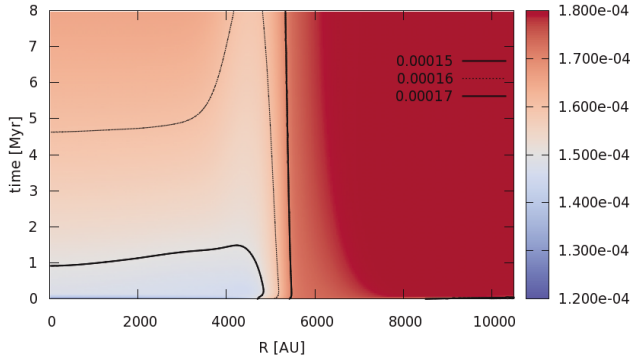


*Fig. 8. Radial and temporal distribution of the relative $H_2O$ abundance $x^*_{H2O}$ in the dust phase. Note the transition radius is located at ~5,000 AU.*

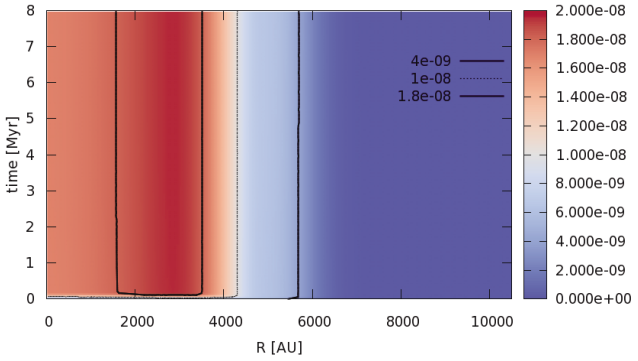


*Fig. 10. Same as Fig. 8, but for $D_2O$. The overall radial gradient is the same as the one of Fig. 9, but the transition radius (~4,000 AU) is located closer to the center.*

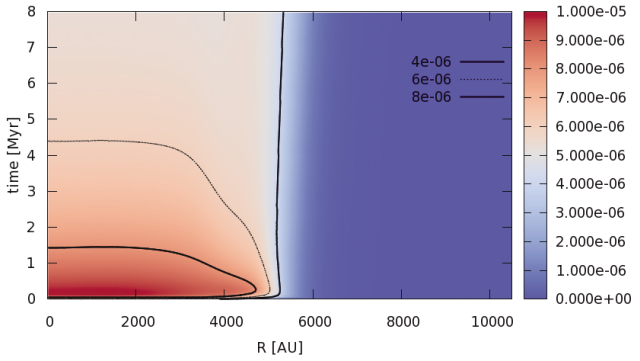


*Fig. 9. Same as Fig. 8, but for HDO. The overall radial gradient is contrary to the one in Fig. 8, and the transition is seen at ~5,000 AU.*

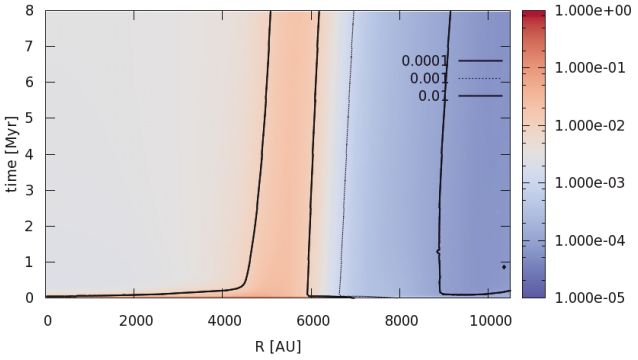


*Fig. 11. Radial and temporal distribution of the abundance ratio $x^*_{HDO}/x^*_{H2O}$ in the dust phase. Note the striking similarity of pattern and magnitude with Fig. 7, leading to the same variation of the abundance ratio in percentage or deuterium enrichment $\delta D$, respectively.*

dance profiles in both phases change slightly with time because of the thermal and UV related evaporation (Semenov, 2006). Recent results have shown that the model of Öberg *et al.* (2009a, b) produces a higher evaporation rate, which conforms better with observations (Caselli *et al.*, 2012). According to Wakelam *et al.* (2014), desorption due to exothermic chemical reactions is even more important but not included in our model. One recognizes a transit range around 5,000 AU given by the condition that the visual extinction $A_V$ is high enough ($A_V$ = 5–6 mag) to completely shield the far UV radiation which otherwise can destroy $H_2O$ molecules or desorb OH species as well as their isotopologues.

There is a small inward motion of the shielding zone caused by an interaction between chemical processes and the inward motion of the dust grains (even for the relatively low UV intensity of the standard ISRF). The transit regions for HDO and $D_2O$ are located in the same radial range but show a lower propensity for inward motion. The variabilities of the D/H and $D_2$/H ratios (Fig. 7) comprise about three to four magnitudes. In addition, both have the maximum in the range of 5,000 AU.

The distributions of the ratios $x^*_{HDO}/x^*_{H2O}$ and $x^*_{D2O}/x^*_{H2O}$ are characterized for $t$ > 1–2 Myr by small time and clear radial variations just as the relative abundances themselves. The $H_2O$ abundances in the inner core are slightly lower while the deuterated species present the lower values in the outer core range (Figs. 9 and 10). Further we should mention that the temporal evolution of $x_{H2O}$ and $x_{HDO}$ in the inner core proceeds contrastively and that $x_{D2O}$ stays relatively constant with time. If one considers the chemical reactions in Eq. (18) one sees that the formation of $H_2O$ on the dust surfaces is driven primarily by the abundance of O which cannot be destroyed by UV radiation, while the formation of HDO and $D_2O$ depends more on $O_2$ or even $O_3$ (Minissale *et al.*, 2013). Models for the corresponding reaction rates and for the quantum tunneling of O (Jing *et al.*, 2012; Chaabouni *et*

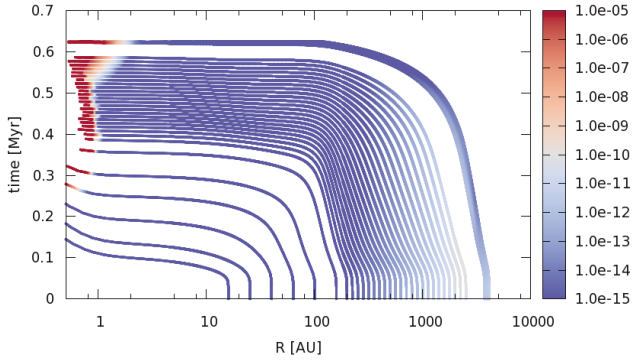


*Fig. 12. Radial and temporal relative abundance distribution $x_{H2O}$ of the gas phase. The light blue color at the outer HCZ range indicates the start of thermal desorption.*

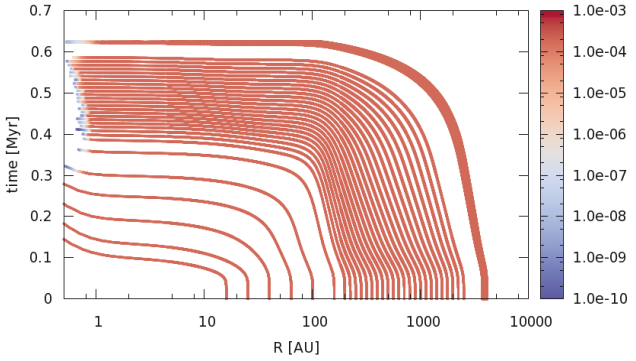


*Fig. 13. Same as Fig. 12 but for the dust phase. The white-bluish color indicates the region with substantial depletion of water ice.*

*al*., 2012; Minissale *et al*., 2013) are derived partly based on the formation model of $H_2$, HD, and $D_2$ in the ice phase (Cazaux and Tielens, 2004). In addition, the gas phase $O_2$, also needed for the $O_3$ formation, is more abundant in the inner region of the core than in the outer region.

A comparison of Fig. 7 with Fig. 11 shows that the D/H ratios in both phases have very similar profiles and variability ranges. However, in the dust phase, the radial profiles of $x^*_{H2O}$ differ clearly from those of $x^*_{HDO}$ and $x^*_{D2O}$. The decreases of the HDO and $D_2O$ abundance below $10^{-6}$ and $10^{-8}$ at $r > 6{,}000$ AU, respectively, in contrast to the small increase of the $H_2O$ abundance (Figs. 8, 9, and 10) reflect the destruction of gas phase $O_2$ by far UV photons. Of course, OH is also dissociated, but can be formed much more easily on the dust surface, again. Thus, one realizes that the profile of the visual extinction influences the abundances of dust phase HDO and $D_2O$ more strongly and contrary to the dust phase $H_2O$ because of the different formation mechanisms (Eq. (18)).

*Formation of $H_2O$ and isotopologues in the collapsing core*

Generally, the gas phase of our collapsing core is chemically influenced by the desorption of volatiles like $H_2O$ or $CH_3OH$, super-volatiles like $CO_2$ or $CH_4$ (Belton, 2010), and the UV radiation entering the core from the outer boundary. If one travels on a Lagrange path into the core center, four chemical zones appear successively. They do not necessarily agree in their boundaries with the density zones presented earlier (see Subsection "The collapsing cloud core"). However, in the same way as the density zones, the chemical zones have time dependent boundaries influenced by the UV radiation and the increasing temperature due to the collapse. At the beginning of the collapse, the ice remains chemically unchanged and is transported with the gas flow into the inner region of the core. If the temperature reaches ~30 K the $CO/H_2O$ ratio drops quickly to $\sim 10^{-4}$, i.e., CO joins the gas phase while water is still locked-up in the dust. Based on the UV radiation and the thermal desorption the four zones are characterized as follows:

1. The photo-dominated zone reaching about 4–6 $A_V$ into the core;

2. The gas-depleted zone mainly influenced by cosmic rays and marginally by UV radiation in its outer part; the temperature at its inner boundary (7–10 AU) is high enough for the thermal desorption of CO (~30 K) denoted as a super ice line (SIL);

3. The transition zone with a gas phase enriched by the super-volatiles and located between the SIL and the radius (1–2 AU) where the temperature is high enough for thermal desorption of $H_2O$, which is denoted as water ice line (WIL); and

4. The hot corino zone between WIL and the dust destruction line, where the temperature is higher than the maximum condensation temperature of the minerals found in the SN.

Concerning these chemical zones, the huge part of the collapsing core belongs to the gas-depleted zone. The chemically interesting zones are the transition and the hot corino zone (HCZ). However, near the inner boundary of the HCZ, the jet forming region is located (Ramsey and Clarke, 2011) since the dust destruction causes the injection of metals into the gas phase. The related increase of the degree of ionisation drives the magnetic interaction between a T-Tauri star and a rotating disk. Nevertheless, we are primarily interested in finding the initial chemical abundances of the planet forming disk range, i.e., the initial values of the last stage of our SN-model so far does not consider jets. Hence we can restrict the complete region of the chemical evolution during the collapse to an interval $r \in I_R = [0.1 \text{ AU}, R_{CE}]$ with $R_{CE} \leq 4{,}000$ AU. Based on this restriction we have selected a set of Lagrangian paths and calculate the chemical evolution of

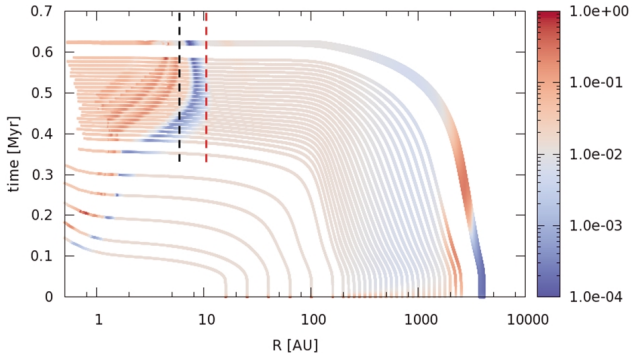


*Fig. 14. Radial and temporal distribution of $x_{HDO}/x_{H2O}$ in the gas phase. We find $x_{HDO}/x_{H2O} \in [10^{-3}, 0.1]$ at 1 AU and $x^*_{HDO}/x^*_{H2O} \in [0.03, 0.05]$ for the dust phase. The related intervals of deuterium enrichment values are $\delta D$ (‰) ∈ [2,200; 320,000] and $\delta D$ (‰) ∈ [95,200; 159,000].*

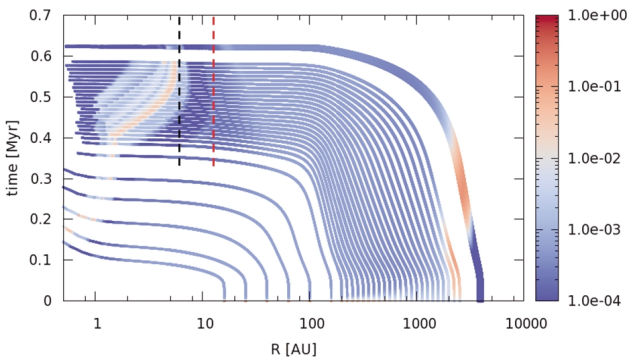


*Fig. 15. Same as Fig. 14, but for $x_{D2O}/x_{H2O}$. At 1 AU, we obtain $x_{D2O}/x_{H2O} \in [3 \times 10^{-6}, 5 \times 10^{-3}]$.*

the related gas pocket along each of these paths. Thereby, we obtain the relative chemical abundances just as for the quasi-stationary core $x_{H2O}$, $x_{HDO}$, $x_{D2O}$, and $x^*_{H2O}$, $x^*_{HDO}$, $x^*_{D2O}$ for the gas and dust phase, respectively.

Figure 12 illustrates that the HCZ is related to the region in which water is enriched due to its desorption from the icy dust mantles, while Fig. 13 presents the corresponding pattern of the $H_2O$ abundance $x^*_{H2O}$ for the dust phase. Both figures show that for early collapse times the WIL is found closer to the core centre, while at late times the WIL moves further out due to the increasing temperature. Zooming into Fig. 12 and considering the interval $0.6 < t < 0.625$, one finds indeed a relatively broad range of WIL locations given by 1.5 AU $< r_{WIL} <$ 2.25 AU, where $r_{WIL}$ denotes the radial position of the WIL.

The interval corresponds to the region between Mars and the inner Main Belt boundary and the maximum relative water abundance is ~$1.7 \times 10^{-4}$. However, a zoom-in of Fig. 13 shows that significant depletion of ice phase water, $x^*_{H2O,dpl} \sim 0.1\ x^*_{H2O,udpl}$, (*dpl* abbreviated for depleted and *udpl* for undepleted) occurs for $r \leq 1$ AU. Indeed one finds that the minimum relative abundance is $1.1 \times 10^{-10}$, while the maximum is $1.8 \times 10^{-4}$. The available thermal energy in the outer range of the HCZ is not high enough to produce large amounts of gas phase water via hot neutral reactions (Eq. (17)). These reactions can proceed efficiently only beyond the white line in Fig. 3, i.e., if $0.1 \leq r \leq 0.8$ AU. At the end of the collapse and for $r$ = 1 AU, the maximum gas and ice phase abundances are quite similar:

$$\max\left(x_{H2O}\right) = 1.2 \times 10^{-4} \quad \text{and} \quad \max\left(x^*_{H2O}\right) = 1.6 \times 10^{-4}.$$

However, the ice phase minimum violates our criterion for a significant ice phase depletion because of $\min(x^*_{H2O}) = 4.8 \times 10^{-5}$, which tells us that the desorption process is not finished in the HCZ and will continue in the disk phase. Since $R_E$ is lower than the complete core radius, $R_C$, the abundances presented in Figs. 12 and 13 originated mainly from the gas-depleted and the transition zone. Accordingly the water ice on the surface of dust grains as well as the one in the gas phase remain unchanged until the corresponding gas pockets reach the IL. Hence, our Lagrange paths symbolize large-scale water inflows at super-sonic velocities (Fig. 5).

The abundance ratios of the HDO and $D_2O$ molecules $x_{HDO}/x_{H2O}$ and $x_{D2O}/x_{H2O}$, of the gas phase, are shown in Figs. 14 and 15. Beyond the super ice line SIL, most of the gas pockets on the Lagrange paths have a slowly varying ratios in both phases. One obtains for the gas phase $x_{HDO}/x_{H2O} \sim 0.01$ and $x_{D2O}/x_{H2O} \sim 0.003$ in the gas-depleted zone.

For the ice phase we obtaine $x^*_{HDO}/x^*_{H2O} \sim 0.04$ and $x^*_{D2O}/x^*_{H2O} \sim 10^{-4}$ with a much lower variability in the same zones. Concerning the deuterium enrichment one gets $\delta D$ = 31,050‰ for the gas phase and an even larger value $\delta D^*$ = 127,200‰ for the dust phase. For the transition zone, one realizes that the gas phase ratios $x_{HDO}/x_{H2O}$ and $x_{D2O}/x_{H2O}$, in contrast to the related abundances, start changing after the gas pocket has reached the its outer boundary which is equivalent to the SIL. For both gas phase abundance ratios, $x_{HDO}/x_{H2O}$ and $x_{D2O}/x_{H2O}$, in the inner transition zone ($r \leq 7$ AU), an interesting pattern is seen from Figs. 14 and 15 shown as a first decrease and a subsequent increase of them. This decrease/increase pattern repeats somehow if one moves further inwards. The outer pattern of $x_{HDO}/x_{H2O}$ shows a strong variation since it decreases from ~0.01 to less than $10^{-3}$ and increases to 0.3–0.5, in total 2.5 magnitudes. The more inner pattern are smoother and vanish finally. In case of $x_{D2O}/x_{H2O}$, the ratio drops from $10^{-3}$ to $10^{-4}$ and rises to 0.03, i.e., about 2.5 magnitudes as well. It seems that these oscillations

seen in the abundamce ratios enlighten slight differences in the abundance profiles of HDO and $D_2O$ with respect to the related profile of $H_2O$. In addition, one has to note that in the transition zone the desorption of water and its isotopologues starts very slowly and initially does not produce molecule abundances higher than those produced by gas chemistry. Keeping this in mind, the oscillations in the Figs. 14 and 15 are a very natural phenomenon.

## Conclusions and Outlook

*Conclusions*

Water has been formed in large abundances ($1.8 \times 10^{-4}$) and with a very small radial variability in the cold quasi-stationary core, which is the first stage of our SN-model (Fig. 1). These large amounts are locked-up as ice mantles on the surface of the dust grains (Fig. 8). The gas phase abundance of water depends on the non-thermal desorption efficiency of $H_2O$ molecules from the ice phase. Its maximum ($\sim 10^{-10}$) occurs in the middle core region (Fig. 6) while the minimum is located at its outer boundary where desorbed water molecules dissociate because of the far UV flux from the ISRF entering the partially shielded core from outside. Since both gas- and dust-phase water form on cold grain surfaces or by ion molecule reactions with a very low efficiency in the cold gas phase, the related profiles of the D/H ratios ($x_{HDO}/x_{H2O}$ and $x^*_{HDO}/x^*_{H2O}$) in both phases are almost equal (Figs. 7 and 11). The fairly large variability of these profiles is seen comparing the ratios between 0.001 ($\delta D \sim \delta D^* \sim$ 2,200‰) and 0.01 ($\delta D \sim \delta D^* \sim$ 31,000‰) in the inner core and $10^{-4}$ ($\delta D \sim -680$‰) in the outer region. It is caused by the influence of the far UV flux since the photo-dissociation of gas phase $O_2$ reduces the amount of adsorbed $O_2$ on the dust surfaces and therefore the formation of dust-phase HDO and $D_2O$. Accordingly the UV radiation of the ISRF can reduce the D/H ratio of water in the dust and gas phase to $10^{-4}$ or to a negative deuterium enrichment value, respectively. The gas phase water abundance of a cold core on the verge to collapse was observed by Caselli *et al*. (2012) from Herschel data of L1544. They derived a relative abundance above $1.7 \times 10^{-10}$ which nearly agrees with the highest values of our simulations. Consequently, we need to improve the used photo-desorption model and include the data reported by Öberg *et al*. (2009a, b). The abundance of ice phase water is hard to be observed, but the derived value of $6 \times 10^{-4}$ added to the observations by Caselli *et al*. (2012) is comparable to the observed fractional water abundance towards the Orion hot cores which is a high mass star forming region (Neill *et al*., 2013). Our maximum values $x^*_{H2O} \sim 2 \times 10^{-4}$ is only 1/3 of the estimated or observed abundance, but there are also observations towards the low mass star forming site NGC1333, which are even smaller (Kristensen *et al*., 2010) than our value. The deuterium fractionation of water $x_{HDO}/x_{H2O}$ varies between 0.02% and 8% for the observed regions described in the Introduction, which nearly agrees with the observations.

The chemical abundances obtained from Stage 1 of our SN-model determine the gas and dust-phase composition at the beginning of the core collapse. We derived a semi-analytical model reproducing a cold outside-in collapse to include the next stage of the solar nebula evolution. Comparisons with other collapse simulations (Schönke and Tscharnuter, 2011; Saigo *et al*., 2008) have shown that these models produce a similar radial density distribution but find higher velocities and temperatures in the inner core region. The main important reason for these differences is the use of a polytropic equation of state (11). According to Vaytet *et al*. (2014), there is some interaction between the chemistry and the dynamics mediated by their state equation. This interaction needs to be considered in the future by adding an additional term to Eqs. (4) and (5), and by adding the energy conservation equation to our set of MHD equations (7)–(10). Our collapse model provides radially symmetric time-dependent density, temperature and velocity distributions which are used to compute a large set of Lagrange paths, symbolizing an inflow stream of the gas-dust material. This type of inflow signature was found by Mottram *et al*. (2013) in the observed water transition lines towards proto-stars in order to study the gas flow velocity of collapsing cores. They have found evidence for large-scale super-sonic inflows (compare with Fig. 5) of water with Herschel and determined that these flows occur on a scale between core and envelope, i.e., $3 \times 10^3$–$10^4$ AU for IRAS 15398, L1527, or L1157. For NGC1333-IRAS4A these flows extend over the envelope, i.e., the related scale is $\geq 10^3$. Moreover, based on these observations they suggest an outside-in rather than inside-out collapse in agreement with the model presented here.

Our cold collapsing core with its small hot corino delivers enough energy at 1 AU (located in the HCZ) to increase the relative abundance of gas phase water by thermal desorption to $1.2 \times 10^{-4}$ while the dust phase is only slightly depleted ($0.5 \times 10^{-4}$). In the region between Venus and Mercury the gas phase abundance is even higher ($1.7 \times 10^{-4}$). These data agree with the observed water abundances between $10^{-5}$–$10^{-4}$ in the outflow region of NGC1333 (Kristensen *et al*., 2010). Lower values of $3 \times 10^{-6}$ and $5 \times 10^{-7}$ are found for the middle and envelope region of IRAS 16293-2422 (Parise *et al*., 2005) which could not be reproduced in our model. There seem to be two possible explanations; First of all, IRAS 16293-2422 is a binary protostar at least and perhaps in the disk phase already. Secondly, our model underestimates the radial range of the HCZ and the non-thermal desorption rate. Concerning the related D/H ratio, the related gas and

dust phase ratios $x_{HDO}/x_{H2O}$ and $x^*_{HDO}/x^*_{H2O}$ at 1 AU vary in the interval [0.001, 0.1] and [0.03, 0.05] (or based on the deuterium enrichment: $\delta$D (‰) $\in$ [2,200; 320,000] and $\delta$D* (‰) $\in$ [95,200; 159,300]), respectively. A comparison of these values with observations towards NGC 1333 which vary from 0.003 to 0.08 for IRAS2A and from 0.007 to 0.03 for IRAS4A, shows a fairly well agreement. Aikawa *et al*. (2012) have obtained similar values for their model of the deuterium fractionation of a protostellar core. There is a large variability for the D/H ratio due to oscillations in the transition and outer hot corino zone ($1 < r <$ 10 AU, Fig. 14), but observations will not resolve this. For hot corinos or hot cores the obtained deuteration is slightly too large (Wakelam *et al*., 2014). Indeed for the IRAS 16293-2422 hot corino one gets 0.09% (Persson *et al*., 2013) while for the hot core of NGC 6334 I (Emprechtinger *et al*., 2012), the D/H ratio of 0.02% is even smaller. A source for a de-deuteration could be an OPR ratio between 0.1 and 1 (Pagani *et al*., 2013). Based on their model, Taquet *et al*. (2014) report a maximum decreasing factor of 2.3 for the gas phase water and 27 for the dust phase assuming OPR = 3. A further source could be a cosmic ray ratio higher than $10^{-16}$ (Wakelam *et al*., 2014). Moreover, the temperature and size of the hot corino can increase during the disk phase because of the transition of the young protostar to a T-Tauri star and the related increase of stellar radiation. Indeed recent disk models (Willacy and Woods, 2009; Thi *et al*., 2010; Furuya *et al*., 2013) produced a higher dust and gas temperature in the central plane region of the inner disk and obtained a lower D/H ratio of water in this region.

*Outlook*

As already mentioned, we plan to extend our chemical module by allowing a variable OPR and an improved non-thermal desorption. In addition we will add the disk stage, since water in special regions (near the dust sublimation layer and on the surface of a flaring disk) is destroyed by energetic radiation (Bruderer *et al*., 2009) and re-formed by hot neutral reactions. As a consequence, these processes influence the D/H ratio of water and need to be considered. In addition, the dust sublimation layer (and thus the inner boundary of the HCZ) is located near the outflowing jets (Goicoechea *et al*., 2012) suggesting an extension of the disk model according to the approach of Combet *et al*. (2010).

**Acknowledgments**—This work was supported partly by the Helmholtz Alliance on planetary evolution and life. We are very grateful to Valentine Wakelam and Dmitry Semenov for providing their chemical codes to us. In addition we have very much appreciated the valuable comments of one anonymous reviewer and of Shogo Tachibana.

## References

Aikawa, Y., Herbst, E., Roberts, H. and Caselli, P. (2005) Molecular evolution in collapsing prestellar cores. III. Contraction of a Bonnor-Ebert sphere. *Astrophys. J.* **620**, 330–346.

Aikawa, Y., Wakelam, V., Garrod, R. T. and Herbst, E. (2008) Molecular evolution and star formation: From prestellar cores to protostellar cores. *Astrophys. J.* **674**, 984–996.

Aikawa, Y., Wakelam, V., Hersant, F., Garrod, R. T. and Herbst, E. (2012) From prestellar to protostellar cores. II. Time dependence and deuterium fractionation. *Astrophys. J.* **760**, 40–58.

Albertsson, T., Semenov, D. A., Vasyunin, A. I., Henning, T. and Herbst, E. (2013) New extended deuterium fractionation model: Assessment at dense ISM conditions and sensitivity analysis. *Astrophys. J. Suppl.* **S207**, 27 (29 pp.).

André, P. (2013) The Herschel View of Star Formation. Highlights of Astronomy, Volume 16, XXVIIIth IAU General Assembly, 2012.

Bacmann, A., André, P., Puget, J.-L., Abergel, A., Bontemps, S. and Ward-Thompson, D. (2000) An ISOCAM absorption survey of the structure of pre-stellar cloud cores. *Astron. Astrophys.* **361**, 555–580.

Baraffe, I., Chabrier, G. and Gallardo, J. (2009) Episodic accretion at early stages of evolution of low-mass stars and brown dwarfs: a solution for the observed luminosity spread in HR diagrams? *Astrophys. J. Lett.* **702**, L27–L31.

Barenblatt, G. I. and Zeldovich, Y. B. (1972) Self-similar solutions as intermediate asymtotics. *Annu. Rev. Fluid Mech.* **4**, 285–312.

Battersby, C., Ginsburg, A., Bally, J., Longmore, S., Dunham, M. and Darling, J. (2014) The onset of massive star formation: The evolution of temperature and density structure in an infrared dark cloud. *Astrophys. J.* **787**, 113 (21 pp.).

Belloche, A., Parise, B., Schuller, F., André, P., Bontemps, S. and Menten, K. M. (2011a) Will the starless cores in Chamaeleon I and III turn prestellar? *Astron. Astrophys.* **535**, A2.

Belloche, A., Schuller, F., Parise, B., André, P., Hatschell, J., Jørgensen, J. K., Bontemps, S., Weiß, A., Menten, K. M. and Muders, D. (2011b) The end of star formation in Chameleon I? A LABOCA census of starless and protostellar cores. *Astron. Astrophys.* **527**, A145.

Belton, M. J. S. (2010) Cometary activity, active areas, and a mechanism for collimated outflows on 1P, 9P, and 81P. *Icarus* **210**, 881–897.

Bergin, E. A. and Snell, R. L. (2002) Sensitive limits on the water abundance in cold low-mass molecular cores. *Astrophys. J. Lett.* **581**, L105–L108.

Bergin, E. A., Goldsmith, P. F., Snell, R. L. and Langer, W. D. (1997) The chemical composition and evolution of giant molecular cloud cores: a comparison of observation and theory. *Astrophys. J.* **482**, 285–297.

Bergin, E. A., Maret, S., van der Tak, F. F. S., Alves, J., Carmody, S. M. and Lada, C. J. (2006) The thermal structure of gas in prestellar cores: a case study of barnard 68. *Astrophys. J.* **645**, 369–380.

Boily, C. M. and Lynden-Bell, D. (1995) Self-similar collapse and accretion of radiative gas. *Mon. Not. R. Astron. Soc.* **276**, 133–166.

Boland, W. and de Jong, T. (1984) Hydrostatic models of molecular clouds. II—Steady state models of spherical clouds. *Astrophys. J.* **134**, 87–98.

Bonev, B. P., Mumma, M. J., Villanueva, G. L., Disanti, M. A., Ellis, R. S., Magee-Sauer, K. and Dello Russo, N. (2007) A search for variation in the $H_2O$ Ortho-para ratio and rotational temperature in the inner coma of comet C/2004 Q2 (Machholz). *Astrophys. J. Lett.* **661**, L97–L100.

Bonev, B. P., Villanueva, G. L., Paganini, L., DiSanti, M. A., Gibb, E. L., Keane, J. V., Meech, K. J. and Mumma, M. J. (2013) Evidence for two modes of water release in Comet 103P/Hartley 2: Distribution of column density, rotational temperature, and ortho-para ratio. *Icarus* **222**, 740–751.

Bonnor, W. B. (1956) Boyle's Law and gravitational instability. *Mon. Not. R. Astron. Soc.* **116**, 351.

Brown, N. P. and Hindmarsh, A. C. (1989) Reduced storage matrix methods in stiff ODE systems. *Applied Mathematics and Computation* **31**, 40–91.

Brown, R. D. and Rice, E. H. N. (1986a) Galactochemistry—Part One—Influence of initial conditions on predicted abundances. *Mon. Not. R. Astron. Soc.* **223**, 405.

Brown, R. D. and Rice, E. H. N. (1986b) Galactochemistry—Part Two—Interstellar deuterium chemistry. *Mon. Not. R. Astron. Soc.* **223**, 429.

Bruderer, S., Doty, S. D. and Benz, A. O. (2009) Chemical modeling of young stellar objects. I. Method and benchmarks. *Astrophys. J. Suppl.* **S183**, 179–196.

Caselli, P., Keto, E., Bergin, E. A., Tafalla, M., Aikawa, Y., Douglas, T., Pagani, L., Yıldız, U. A., van der Tak, F. F. S., Walmsley, C. M., Codella, C., Nisini, B., Kristensen, L. E. and van Dishoeck, E. F. (2012) First detection of water vapor in a pre-stellar core. *Astrophys. J. Lett.* **759**, L37 (5 pp.).

Cazaux, S. and Tielens, A. G. G. M. (2004) $H_2$ formation on grain surfaces. *Astrophys. J.* **604**, 222–237.

Cazaux, S., Caselli, P. and Spaans, M. (2011) Interstellar ices as witnesses of star formation: Selective deuteration of water and organic molecules unveiled. *Astrophys. J. Lett.* **741**, L34 (6 pp.).

Ceccarelli, C. (2004) The hot corinos of solar type protostars. *Star Formation in the Interstellar Medium: In Honor of Hollenbach D., McKee C., and Shu F. ASP Conference Proceedings* (Johnstone, D., Adams, F. C., Lin, D. N. C., Neufeld, D. A. and Ostriker, E. C., eds.), *Astron. Soc. Pac. Conf. Ser.* **323**, 195.

Ceccarelli, C., Hollenbach, D. J. and Tielens, A. G. G. M. (1996) Far-infrared line emission from collapsing protostellar envelopes. *Astrophys. J.* **471**, 400–426.

Chaabouni, H., Minissale, M., Manicò, G., Congiu, E., Noble, J. A., Baouche, S., Accolla, M., Lemaire, J. L., Pirronello, V. and Dulieu, F. (2012) Water formation through $O_2$ + D pathway on cold silicate and amorphous water ice surfaces of interstellar interest. *J. Chem. Phys.* **137**, 234706.

Charnley, S. B. (1997) Sulfuretted molecules in hot cores. *Astrophys. J.* **481**, 396–405.

Combet, C., Ferreira, J. and Casse, F. (2010) Dead zones in protostellar disk: the case of jet emitting discs. *Astron. Astrophys.* **519**, A108 (10 pp.).

Commerçon, B., Hennebelle, P., Audit, E., Chabrier, G. and Teyssier, R. (2008) Protostellar collapse: a comparison between smoothed particle hydrodynamics and adaptative mesh refinement calculations. *Astron. Astrophys.* **482**, 371–385.

Coutens, A., Vastel, C., Cazaux, S., Bottinelli, S., Caux, E., Ceccarelli, C., Demyk, K., Taquet, V. and Wakelam, V. (2013) Heavy water stratification in a low-mass protostar. *Astron. Astrophys.* **553**, A75.

Crapsi, A., Caselli, P., Walmsley, M. C. and Tafalla, M. (2007) Observing the gas temperature drop in the high-density nucleus of L 1544. *Astron. Astrophys.* **470**, 221–230.

de Boisanger, C., Helmich, F. P. and Dishoeck, E. F. (1996) The ionization fraction in dense clouds. *Astron. Astrophys.* **310**, 315–327.

Dello Russo, N., Boney, B. P., DiSanti, M. A., Mumma, M. J., Gibb, E. L., Magee-Sauer, K., Barber, R. J. and Tennyson, J. (2005) Water production rates, rotational temperatures, and spin Temperatures in Comet C/1999 H1 (Lee), C/1999 S4, and C/2001 A2. *Astrophys. J.* **621**, 537–544.

Doty, S D., Schoier, F. L. and van Dishoeck, E. F. (2004) Physical-chemical modeling of the low-mass protostar IRAS 16293-2422. *Astron. Astrophys.* **418**, 1021–1034.

Drouart, A., Dubrulle, B., Gautier, D. and Robert, F. (1999) Structure and transport in the solar nebula from constraints on deuterium enrichment and giant planets formation. *Ikarus* **140**(1), 129–155.

Dulieu, F., Amiaud, L., Congiu, E., Filloin, J.-H., Matar, E., Momeni, A., Pirronello, V. and Lemaire, J. L. (2010) Experimental evidence for water formation on interstellar dust grains by hydrogen and oxygen atoms. *Astron. Astrophys.* **512**, A30.

Ebert, R. (1957) Zur Instabilität kugelsymmetrischer Gasverteilungen. *Zeitschrift für Astrophysik* **42**, 263.

Emprechtinger, M., Lis, D. C., Rolffs, D. C., Schilke, P., Monje, R. R., Comito, C., Ceccarelli, C., Neufeld, D. A. and van der Tak, F. F. S. (2012) The abundance, ortho/para ratio, and deuteration of water in the high-mass star forming region NGC 6334 I. *Astrophys. J.* **765**, 13.

Fatuzzo, M., Adams, F. C. and Myers, P. C. (2004) Generalized collapse solutions with nonzero initial velocities for star formation in molecular cloud cores. *Astrophys. J.* **615**, 813–831.

Flower, D. R., Pineau des Forêts, G. and Walmsley, C. M. (2004) Multiply-deuterated species in prestellar cores. *Astron. Astrophys.* **427**, 887–893.

Flower, D. R., Pineau des Forêts, G. and Walmsley, C. M. (2006) The importance of the ortho:papr $H_2$ ratio for the deuteration of molecules during pre-Protostellar collapse. *Astron. Astrophys.* **449**, 621–629.

Franklin, J., Snell, R. L., Kaufmann, M. J., Melnick, G. J., Neufeld, D. A., Hollenbach, D. J. and Bergin, E. A. (2008) SWAS observations of water in molecular outflows. *Astrophys. J.* **674**, 1015–1031.

Furuya, K., Aikawa, Y., Nomura, H., Hersant, F. and Wakelam, V. (2013) Water in protoplanetary disk: Deuteration and turbulent mixing. *Astrophys. J.* **779**, 11 (19 pp.).

Garrod, R. T. and Herbst, E. (2006) Formation of methyl for-

mate and other organic species in the warm-up phase of hot molecular cores. *Astron. Astrophys.* **457**, 927–936.

Garrod, R. T. and Weaver, S. L. (2013) Simulation of hot-core chemistry. *Chemical Reviews Special Issue: Astrochemistry*, 8939–8960.

Gavilan, L., Vidali, G., Lemaire, J. L., Chehrouri, M., Dulieu, F., Fillion, J.-H., Congiu, E. and Chaabouni, H. (2012) Experimental investigation of the ortho/para ratio of newly formed molecular hydrogen on amorphous solid water. *Astrophys. J.* **760**(1), 35 (8 pp.).

Glassgold, A. E. and Langer, W. D. (1976) Abundances of simple oxygen-bearing molecules and ions in interstellar clouds. *Astrophys. J.* **206**, 85–99.

Goicoechea, J. R., Cernicharo, J., Karska, A., Herczeg, G. J., Polehampton, E. T., Wampfler, S. F., Kristensen, L. E., van Dishoeck, E. F., Etxaluze, M., Berné, O. and Visser, R. (2012) The complete far-infrared and submillimeter spectrum of the Class 0 protostar Serpens SMM1 obtained with Herschel Characterizing UV-irradiated shocks heating and chemistry. *Astron. Astrophys.* **548**, A77.

Gong, H. and Ostriker, E. C. (2009) Protostar formation in supersonic flows: growth and collapse of spherical cores. *Astrophys. J.* **699**, 230–244.

Hama, T., Kuwahata, K., Watanabe, N., Kouchi, A., Kimura, Y., Chigai, T. and Pirronello, V. (2012) The mechanism of surface diffusion of H and D atoms on amorphous solid water: Existence of various potential sites. *Astrophys. J.* **757**, 185 (12 pp.).

Hasegawa, T. I. and Herbst, E. (1993) New gas-grain chemical models of quiescent dense interstellar clouds—The effects of $H_2$ tunnelling reactions and cosmic ray induced desorption. *Mon. Not. R. Astron. Soc.* **261**, 83–102.

Hasegawa, T. I., Herbst, E. and Leung, C. M. (1992) Models of gas-grain chemistry in dense interstellar clouds with complex organic molecules. *Astrophys. J. Suppl.* **S82**, 167–195.

Hassel, G. E., Herbst, E. and Garrod, R. T. (2008) Modeling the lukewarm corino phase: Is L 1527 unique? *Astrophys. J.* **681**, 1385–1395.

Herbst, E. and Klemperer, W. (1973) The formation and depletion of molecules in dense interstellar clouds. *Astrophys. J.* **185**, 505–534.

Hincelin, U., Wakelam, V., Commerçon, B., Hersant, F. and Guilloteau, S. (2013) Survival of interstellar molecules to prestellar dense core collapse and early phases of disk formation. *Astrophys. J.* **775**, 44 (11 pp.).

Hiraoka, K., Wada, A., Kitagawa, H., Kamo, M., Unagiike, H., Ueno, T., Sugimoto, T., Enoura, T., Sogoshi, N. and Okazaki, S. (2005) The reactions of H and D atoms with thin films of formaldehyde and methanol at cryogenic temperatures. *Astrophys. J.* **620**, 542–551.

Hollenbach, D. J. and Tielens, A. G. G. M. (1999) Photodissociation regions in the interstellar medium of galaxies. *Rev. Modern Phys.* **71**, 173–230.

Hollenbach, D., Kaufman, M. J., Neufeld, D., Wolfire, M. and Goicoechea, J. R. (2012) The chemistry of interstellar $OH^+$, $H_2O^+$, and $H_3O^+$: Inferring the cosmic-ray ionization rates from observations of molecular ions. *Astrophys. J.* **754**, 105 (22 pp.).

Howe, D. A. and Millar, T. J. (1993) Alternative routes to deuteration in dark clouds. *Mon. Not. R. Astron. Soc.* **262**, 868–880.

Howe, D. A., Millar, T. J., Schilke, P. and Walmsley, C. M. (1994) Observations of deuterated cyanoacetylene in dark clouds. *Mon. Not. R. Astron. Soc.* **267**, 59.

Jansson, K. W. and Johansen, A. (2014) Formation of pebble-pile planetesimals. *Astron. Astrophys.* **570**, A47 (10 pp.).

Jing, D., He, J., Brucato, J. R., Vidali, G., Tozzetti, L. and de Sio, A. (2012) Formation of molecular oxygen and ozone on amorphous silicates. *Astrophys. J.* **756**, 98 (7 pp.).

Jørgensen, J. K. and van Dishoeck, E. F. (2010) Water vapor in the inner 25 AU of a young disk around a low-mass protostar. *Astrophys. J. Lett.* **710**, L72–L76.

Keto, E., Broderick, A. E., Lada, C. J. and Narayan, R. (2006) Oscillations of starless cores. *Astrophys. J.* **652**, 1366–1373.

Keto, E., Rawlings, J. and Caselli, P. (2014) Chemistry and radiative transfer of water in cold, dense clouds. *Mon. Not. R. Astron. Soc.* **440**, 2616–2624.

King, H. E., Stimpfl, M., Deymier, P., Drake, M. J., Catlow, C. R. A., Putnis, A. and de Leeuw, N. H. (2010) Computer simulations of water interactions with low-coordinated forsterite surface sites: Implications for the origin of water in the inner solar system. *Earth Planet. Sci. Lett.* **300**, 11–18.

Kristensen, L. E., Visser, R., van Dishoeck, E. F., Yıldız, U. A., Doty, S. D., Herczeg, G. J., Liu, F.-C., Parise, B., Jørgensen, J. K., van Kempen, T. A., Brinch, C., Wampfler, S. F., Bruderer, S., Benz, A. O., Hogerheijde, M. R., Deul, E., Bachiller, R., Baudry, A., Benedettini, M., Bergin, E. A., Bjerkeli, P., Blake, G. A., Bontemps, S., Braine, J., Caselli, P., Cernicharo, J., Codella, C., Daniel, F., de Graauw, Th., di Giorgio, A. M., Dominik, C., Encrenaz, P., Fich, M., Fuente, A., Giannini, T., Goicoechea, J. R., Helmich, F., Herpin, F., Jacq, T., Johnstone, D., Kaufman, M. J., Larsson, B., Lis, D., Liseau, R., Marseille, M., McCoey, C., Melnick, G., Neufeld, D., Nisini, B., Olberg, M., Pearson, J. C., Plume, R., Risacher, C., Santiago-García, J., Saraceno, P., Shipman, R., Tafalla, M., Tielens, A. G. G. M., van der Tak, F., Wyrowski, F., Beintema, D., de Jonge, A., Dieleman, P., Ossenkopf, V., Roelfsema, P., Stutzki, J. and Whiborn, N. (2010) Water in low-mass star-forming regions with Herschel HIFI spectroscopy of NGC 1333. *Astron. Astrophys.* **521**, L30.

Kristensen, L. E., Amiaud, L., Fillion, J.-H., Dulieu, F. and Lemaire, J.-L. (2011) $H_2$, HD, and $D_2$ abundances on ice-covered dust grains in dark clouds. *Astron. Astrophys.* **527**, A44.

Krumholz, M. R., Klein, R. I. and McKee, C. F. (2007) Radiation-hydrodynamic simulations of collapse and fragmention in massive protostellar cores. *Astrophys. J.* **656**, 959–979.

Kupper, S. (2014) Influence of dust properties on the chemical abundances and D/H ratio of important prebiotic compounds in the Solar Nebula. Dr. Sci. Thesis, Tech. Univ. Braunschweig (in German) (in prep.).

Lada, C. J. (2006) Stellar multiplicity and the initial mass function: Most stars are single. *Astrophys. J. Lett.* **640**, L63–L66.

Langer, W. D. and Graedel, T. E. (1989) Ion-molecule chemis-

try of dense interstellar clouds—Nitrogen-, oxygen-, and carbon-bearing molecule abundances and isotopic ratios. *Astrophys. J. Suppl.* **S69**, 241–269.

Larson, R. B. (1969) Numerical calculations of the dynamics of collapsing proto-star. *Mon. Not. R. Astron. Soc.* **145**, 27.

Larsson, M., Geppert, W. D. and Nyman, G. (2012) Ion chemistry in space. *Rep. Prog. Phys.* **75**, 066901 (75 pp.).

Launhardt, R., Stutz, A. M., Schmiedeke, A., Henning, Th., Krause, O., Balog, Z., Beuther, H., Birkmann, S., Hennemann, M., Kainulainen, J., Khanzadyan, T., Linz, H., Lippok, N., Nielbock, M., Pitann, J., Ragan, S., Risacher, C., Schmalzl, M., Shirley, Y. L., Stecklum, B., Steinacker, J. and Tackenberg, J. (2013) The Earliest Phase of Star formation (EPoS): a Herschel key project. The thermal structure of low-mass molecular cloud cores. *Astron. Astrophys.* **551**, A98 (35 pp.).

LeDrew, G. (2001) The real starry sky. *J. Roy. Astron. Soc. Canada* **95**, 32–33.

Lee, H.-H., Bettens, R. P. A. and Herbst, E. (1996) Fractional abundances of molecules in dense interstellar clouds: A compendium of recent model results. *Astron. Astrophys. Suppl.* **S119**, 111–114.

Lee, J.-E., Bergin, E. A. and Evans, N. J., II (2004) Evolution of chemistry and molecular line profiles during ptotostellar collapse. *Astrophys. J.* **517**, 360–383.

Lodders, K. (2003) Solar system abundances and condensation temperatures of the elements. *Astrophys. J.* **591**, 1220–1247.

Lodders, K., Palme, H. and Gail, H. P. (2009) *Landolt-Bórnstein, Astronomy, Astrophysics and Cosmology* Vol. **VI/4B**, Chap. 4.4, 560–630, Springer Verlag.

Lufkin, E. A. and Hawley, J. F. (1993) The piecewise-linear predictor-corrector code—A Lagrangian-remap method for astrophysical flows. *Astrophys. J. Suppl.* **S88**, 569–588.

Machida, M. N., Inutsuka, S. and Matsumoto, T. (2007) Magnetic fields and rotations of protostars. *Astrophys. J.* **670**, 1198–1213.

Maret, S., Ceccarelli, C., Caux, E., Tielens, A. G. G. M., Jørgensen, J. K., van Dishoeck, E., Bacmann, A., Castets, A., Lefloch, B., Loinard, L., Parise, B. and Schöier, F. L. (2004) The $H_2CO$ abundance in the inner warm regions of low mass protostellar envelopes. *Astron. Astrophys.* **416**, 577–594.

Maret, S., Bergin, E. A. and Lada, C. J. (2007) Using chemistry to unveil the kinematics of starless cores: Complex radial motions in barnard 68. *Astrophys. J. Lett.* **670**, L25–L28.

Masunaga, H. and Inutsuka, S.-I. (2000) A radiation hydrodynamic model for protostellar collapse. II. The second collapse and the birth of a protostar. *Astrophys. J.* **531**, 350–365.

Masunaga, H., Miyama, S. M. and Inutsuka, S.-I. (1998) A radiation hydrodynamic model for protostellar collapse. I. The first collapse. *Astrophys. J.* **495**, 346–369.

Matar, E., Congiu, E., Dulieu, F., Momeni, A. and Lemaire, J. L. (2008) Mobility of D atoms on porous amorphous water ice surfaces under interstellar conditions. *Astron. Astrophys.* **492**, L17–L20.

Matar, E., Bergeron, H., Dulieu, F., Chaabouni, H., Accolla, M. and Lemaire, J. L. (2010) Gas temperature dependent sticking of hydrogen on cold amorphous water ice surfaces of interstellar interest. *J. Chem. Phys.* **133**, 104507.

Mathis, J. S., Rumpl, W. and Nordsieck, K. H. (1977) The size distribution of interstellar grains. *Astrophys. J.* **217**, 425–433.

Meng, F., Wu, Y. and Liu, T. (2013) Mapping study of 71 Planck cold clumps in the Taurus, Perseus, and California Complexes. *Astrophys. J.* **209**, 37 (23 pp.).

Millar, T. J., Bennett, A. and Herbst, E. (1989) Deuterium fractionation in dense interstellar clouds. *Astrophys. J.* **340**, 906–920.

Minissale, M., Congiu, E., Baouche, S., Chaabouni, H., Moudens, A. and Dulieu, F. (2013) Quantum tunneling of oxygen atoms on very cold surfaces. *Phys. Rev. Lett.* **111**, 053201.

Mokrane, H., Chaabouni, H., Accolla, M., Congiu, E., Dulieu, F., Chehrouri, M. and Lemaire, J. L. (2009) Experimental evidence for water formation via ozone hydrogenation on dust grains at 10 K. *Astrophys. J. Lett.* **705**, L195–L198.

Morbidelli, A., Lunine, J. I., O'Brien, D. P., Raymond, S. N. and Walsh, K. J. (2012) Building terrestrial planets. *Ann. Rev. Earth Planet. Sci.* **40**, 251–275.

Mottram, J. C., van Dishoeck, E. F., Schmalzl, M., Kristensen, L. E., Visser, R., Hogerheijde, M. R. and Bruderer, S. (2013) Waterfalls around protostars. Infall motions toward Class 0/1 envelopes as probed by water. *Astron. Astrophys.* **558**, A126.

Neill, J. L., Wang, S., Bergin, E. A., Crockett, N. R., Favre, C., Plume, R. and Melnick, G. J. (2013) The Abundance of $H_2O$ and HDO in Orion K1 from Herschel/HIFI. *Astrophys. J.* **770**, 142 (18 pp.).

Nejad, L. A. M. and Wagenblast, R. (1999) Time dependent chemical models of spherical dark clouds. *Astron. Astrophys.* **350**, 204–229.

Öberg, K. I., Dishoeck, E. F. and Linnartz, H. (2009a) Photodesorption of ices I: CO, $N_2$ and $CO_2$. *Astron. Astrophys.* **496**, 281–293.

Öberg, K. I., Dishoeck, E. F. and Linnartz, H. (2009b) Photodesorption of ices II: $H_2O$ and $D_2O$. *Astrophys. J.* **693**, 1208–1209.

Osamura, Y., Roberts, H. and Herbst, E. (2005) The gas-phase deuterium fractionation of formaldehyde. *Astrophys. J.* **621**, 348–358.

Pagani, L., Lesffre, P., Jorfi, M., Honvault, P., González-Lezana, T. and Faure, A. (2013) Ortho-$H_2$ and the age of prestellar cares. *Astron. Astrophys.* **551**, A38.

Parise, B., Caux, E., Castets, A., Ceccarelli, C., Loinard, L., Tielens, A. G. G. M., Bacmann, A., Cazaux, S., Comito, C., Helmich, F., Kahane, C., Schilke, P., van Dishoeck, E., Wakelam, V. and Walters, A. (2005) HDO abundance in the envelope of the solar-type protostar IRAS 16293-2422. *Astron. Astrophys.* **431**, 547–554.

Penston, M. V. (1969) Dynamics of self-gravitating gaseous spheres-II. Collapses of gas spheres with cooling and the behaviour of polytropic gas spheres. *Mon. Not. R. Astron. Soc.* **145**, 457.

Persson, M. V., Jørgensen, J. K. and van Dishoeck, E. F. (2013) Warm water deuterium fractionation in IRAS 16293-2422 The high-resolution ALMA and SMA view. *Astron.*

*Astrophys*. **549**, L3.
Prasad, S. S. and Huntress, W. T., Jr. (1980) A model for gas phase chemistry in interstellar clouds I—The basic model, library of chemical reactions, and chemistry among C, N, and O compounds. *Astrophys. J. Suppl*. **S43**, 1–35.
Ramsey, J. P. and Clarke, D. A. (2011) Simulating protostellar jets simultaneously at launching and observational scales. *Astrophys. J. Lett*. **728**, L11 (6 pp.).
Regev, O. and Shaviv, G. (1981) Formation of protostars in collapsing, rotating, turbulent clouds. *Astrophys. J*. **245**, 934–959.
Rodgers, S. D. and Charnley, S. B. (2003) Chemical evolution in protostellar envelopes: Cocoon chemistry. *Astrophys. J*. **585**, 355–371.
Roueff, E., Parise, B. and Herbst, E. (2007) Deuterium fractionation in warm dense interstellar clumps. *Astron. Astrophys*. **464**, 245–252.
Saigo, K., Tomisaka, K. and Matsumoto, T. (2008) Evolution of first cores and formation of stellar cores in rotating molecular cloud cores. *Astrophys. J*. **674**, 997–1014.
Schnee, S., Brunetti, N., Di Francesco, J., Caselli, P., Friesen, R., Johnstone, D. and Pon, A. (2013) Correlating infall with deuterium fractionation in dense cores. *Astrophys. J*. **777**, 121 (10 pp.).
Schönke, J. and Tscharnuter, W. M. (2011) Protostellar collapse of rotating cloud cores. Covering the complete first accretion period of the stellar core. *Astron. Astrophys*. **526**, A139.
Semenov, D. (2006) Dust and Gas in Protoplanetary Disk. Dr. Sci. Thesis, Friedrich-Schiller-Universität Jena.
Semenov, D. and Wiebe, D. (2011) Chemical evolution of turbulent protoplanetary disks and the solar nebula. *Astrophys. J. Suppl*. **S196**, 37.
Semenov, D., Hersant, F., Wakelam, V., Dutrey, A., Chapillon, E., Guilloteau, St., Henning, Th., Launhardt, R., Piétu, V. and Schreyer, K. (2010) Chemistry in disks. IV. Benchmarking gas-grain chemical models with surface reactions. *Astron. Astrophys*. **522**, A42.
Shu, F. H. (1977) Self-similar collapse of isothermal spheres and star formation. *Astrophys. J*. **214**, 488–497.
Sipilä, O. (2012) Radial molecular abundances and gas cooling in starless cores. *Astron. Astrophys*. **543**, 11.
Smith, I. W. M., Herbst, E. and Chang, Q. (2004) Rapid neutral-neutral reactions at low temperatures: a new network and first results for TMC-1. *Mon. Not. R. Astron. Soc*. **350**, 323–330.
Stahler, S. W. and Palla, F. (2004) *The Formation of Stars*. Wiley-VCH Verlag GmbH & Co. KGaA, Weinheim.
Stahler, S. W., Korycansky, D. G., Brothers, M. J. and Touma, J. (1994) The early evolution of protostellar disk. *Astrophys. J*. **431**, 341–358.
Stamatellos, D., Whitworth, A. P. and Hubber, D. A. (2012) Episodic accretion, protostellar radiative feedback, and their role in low-mass star formation. *Mon. Not. R. Soc*. **407**, 1182–1193.
Stutz, A., Launhardt, R., Linz, H., Krause, O., Henning, T., Kainulainen, J., Nielbock, M., Steinacker, J. and André, P. (2010) Dust-temperature of an isolated star-forming cloud: Herschel observations of the Bok globule CB244. *Astron. Astrophys*. **518**, L87.
Takeuchi, T. and Lin, D. N. C. (2002) Radial flow of dust particles in accretion disks. *Astrophys. J*. **581**(2), 1344–1355.
Takeuchi, T. and Lin, D. N. C. (2005) Attenuation of millimeter emission from circumstellar disks induced by the rapid dust accretion. *Astrophys. J*. **623**, 482–492.
Takeuchi, T., Clarke, C. J. and Lin, D. N. C. (2005) The differential lifetimes of protostellar gas and dust disks. *Astrophys. J*. **627**, 286–292.
Taquet, V., Lopez-Sepulcre, A., Ceccarelli, C., Neri, R., Kahane, C., Coutens, A. and Vastel, C. (2013) Water deuterium fractionation in the inner regions of two solar-types protostars. *Astrophys. J. Lett*. **768**, L29 (6 pp.).
Taquet, V., Charnley, S. B. and Sipilä, O. (2014) Multilayyer formation and evaporation of deuterated ices in prestellar and protostellar cores. *Astrophys. J*. **791**, 1 (20 pp.).
Thi, W.-F., Woitke, P. and Kamp, I. (2010) Warm non-equilibrium gas phase chemistry as a possible origin of high $HDO/H_2O$ ratios in hot and dense gases: application to inner protoplanetary discs. *Mon. Not. R. Astron. Soc*. **407**, 232–246.
Tielens, A. G. G. M. (1983) Surface chemistry of deuterated molecules. *Astron. Astrophys*. **119**, 177–184.
Tielens, A. G. G. M. (2005) *The Physics and Chemistry of the Interstellar Medium*. Cambridge University Press.
Tobin, J. J., Hartmann, L., Chiang, H.-F., Wilner, D. J., Looney, L. W., Loinard, L., Calvet, N. and Dàlessio, P. (2013) Modeling the resolved disk around the class 0 protostar L 1527. *Astrophys. J*. **771**, 48 (19 pp.).
Tornow, C., Gast, P., Pelivan, I., Kupper, S., Kührt, E. and Motschmann, U. (2014a) Water formation in early solar nebula: I. Quasi-stationary cloud core. *Planet. Space Sci*. **98**, 216–232.
Tornow, C., Gast, P., Motschmann, U., Kupper, S., Kührt, E. and Pelivan, I. (2014b) Water formation in early solar nebula: II. Collapsing cloud core. *Planet. Space Sci*. **98**, 233–253.
Troscomp, N., Faure, A., Maret, S., Cecarelli, C., Hily-Blant, P. and Wiesenfeld, L. (2009) Constraining the ortho-to-para ratio of $H_2$ with anomalous $H_2CO$ absorption. *Astron. Astrophys*. **506**, 1243–1247.
Turner, B. E. (1993) On the nature of the molecular cores in high-latitude cirrus clouds. III. CO observations and tests of CO chemistry models. *Astrophys. J*. **405**, 229–248.
Turner, B. E. (2000) A Common gas-phase chemistry for diffuse, translucent, and dense clouds? *Astrophys. J*. **542**, 837–860.
van Weeren, R. J., Brinch, C. and Hogerheijde, M. R. (2009) Modeling the chemical evolution of a collapsing prestellar core in two spatial dimensions. *Astron. Astrophys*. **497**, 773–787.
Vaytet, N., Tomida, K. and Chabrier, G. (2014) On the role of the $H_2$ ortho:para ratio in gravitational collapse during star formation. *Astron. Astrophys*. **563**, A85.
Visser, A. E., Richer, J. S. and Chandler, C. J. (2002) Completion of a SCUBA survey of Lynds dark clouds and implication fpr low-mass star formation, *Astron. J*. **124**, 2756–2789.
Visser, R., van Dishoeck, E. F., Doty, S. D. and Dullemond, C. P. (2009) The chemical history of molecules in cirkumstellar disk I. Ices. *Astron. Astrophys*. **495**, 881–897.

Visser, R., Doty, S. D. and van Dishoeck, E. F. (2011) The chemical history of molecules in circumstellar disks. II. Gas-phase species. *Astron. Astrophys.* **534**, A132.

Visser, R., Jørgensen, J. K., Kristensen, L. E., van Dishoeck, E. F. and Bergin, E. A. (2013) Hot water in the inner 100 AU of the class 0 protostar NGC1333 IRAS2A. *Astrophys. J.* **769**, 19 (11 pp.).

Wakelam, V., Herbst, E. and Selsis, F. (2006) The effect of uncertainties on chemical models of dark clouds. *Astron. Astrophys.* **451**, 551–562.

Wakelam, V., Smith, I. W. M., Herbst, E., Troe, J., Geppert, W., Linnartz, H., Öberg, K., Roueff, E., Agúndez, M., Pernot, P., Cuppen, H. M., Loison, J. C. and Talbi, D. (2010) Reaction networks for interstellar chemical modelling: improvements and challenges. *Space Sci. Rev.* **156**, 13–72.

Wakelam, V., Herbst, E., Loison, J.-C., Smith, I. W. M., Chandrasekaran, V., Pavone, B., Adams, N. G., Bacchus-Montabonel, M.-C., Bergeat, A., Béroff, K., Bierbaum, V. M., Chabot, M., Dalgarno, A., van Dishoeck, E. F., Faure, A., Geppert, W. D., Gerlich, D., Galli, D., Hébrard, E., Hersant, F., Hickson, K. M., Honvault, P., Klippenstein, S. J., Le Picard, S., Nyman, G., Pernot, P., Schlemmer, S., Selsis, F., Sims, I. R., Talbi, D., Tennyson, J., Troe, J., Wester, R. and Wiesenfeld, L. (2012) A Kinetic Database for Astrochemistry (KIDA). *Astrophys. J. Suppl.* **S199**, 21 (10 pp.).

Wakelam, V., Vastel, C., Aikawa, Y., Coutens, A., Bottinelli, S. and Caux, E. (2014) Chemical modelling of water deuteration in IRAS16293-2422. *Mon. Not. R. Astron. Soc.* **445**, 2854–2871.

Walmsley, C. M., Flower, D. R. and Pineau des Forêts, G. (2004) Complete depletion in prestellar cores. *Astron. Astrophys.* **418**, 1035–1043.

Whitworth, A. P. and Bate, M. R. (2002) Dust dynamics in dense molecular cores. *Mon. Not. R. Astron. Soc.* **333**, 679–686.

Whitworth, A. and Sommers, D. (1985) Self-similar condensation of spherically symmetric self-gravitating isothermal gas clouds. *Mon. Not. R. Astron. Soc.* **214**, 1–25.

Willacy, K. (2007) The chemistry of multiply deuterated molecules in protoplanetary disks. I. The outer disk. *Astrophys. J.* **660**, 441–460.

Willacy, K. and Woods, P. M. (2009) Deuterium chemistry in protoplanetary Disks. II. The inner 30 AU. *Astrophys. J.* **703**, 479–499.

Williams, J. P. and Cieza, L. A. (2011) Protoplanetary disk and their evolution. *Ann. Rev. Astron. Astrophys.* **49**, 67–117.

Yang, L., Ciesla, F. J. and Alexander, C. M. O'D. (2013) The D/H ratio of water in the solar nebula during its formation and evolution. *Ikarus* **226**, 256–267.

Zubko, V., Dwek, E. and Arendt, R. G. (2004) Interstellar dust models consistent with extinction, emission, and abundance constraints. *Astrophys. J. Suppl.* **S152**, 211–249.

Zucconi, A., Walmsley, C. M. and Galli, D. (2001) The dust temperature distribution in prestellar cores. *Astron. Astrophys.* **376**, 650–662.